Available online at www.sciencedirect.com
ScienceDirect
Comput. Methods Appl. Mech. Engrg. 405 (2023) 115866
Computer methods in applied mechanics and engineering
www.elsevier.com/locate/cma

On the influence of the nonlinear term in the numerical approximation of Incompressible Flows by means of proper orthogonal decomposition methods

Bosco García-Archilla[a,1], Julia Novo[b,*,2], Samuele Rubino[c,3]

[a] *Departamento de Matemática Aplicada II, Universidad de Sevilla, Sevilla, Spain*
[b] *Departamento de Matemáticas, Universidad Autónoma de Madrid, Spain*
[c] *Department EDAN & IMUS, Universidad de Sevilla, Spain*

Received 29 March 2022; received in revised form 19 December 2022; accepted 20 December 2022
Available online 30 December 2022

Abstract

We consider proper orthogonal decomposition (POD) methods to approximate the incompressible Navier–Stokes equations. We study the case in which one discretization for the nonlinear term is used in the snapshots (that are computed with a full order method (FOM)) and a different discretization of the nonlinear term is applied in the POD method. We prove that an additional error term appears in this case, compared with the case in which the same discretization of the nonlinear term is applied for both the FOM and the POD methods. However, the added term has the same size as the error coming from the FOM so that the rate of convergence of the POD method is barely affected. We analyze the case in which we add grad–div stabilization to both the FOM and the POD methods because it allows to get error bounds with constants independent of inverse powers of the viscosity. We also study the case in which no stabilization is added. Some numerical experiments support the theoretical analysis.

MSC: 35Q30; 65M12; 65M15; 65M20; 65M60; 65M70; 76B75

Keywords: Navier–Stokes equations; Proper orthogonal decomposition; Nonlinear term discretization; Grad–div stabilization

1. Introduction

The computational cost of direct numerical simulations can be reduced by using reduced order models. The proper orthogonal decomposition (POD) method is based on a reduced basis that is computed using snapshots coming from a full order method (FOM). In this paper, we study the numerical approximation of incompressible flows with POD methods.

* Corresponding author.
E-mail addresses: bosco@esi.us.es (B. García-Archilla), julia.novo@uam.es (J. Novo), samuele@us.es (S. Rubino).
[1] Research is supported by Spanish MCINYU under grants PGC2018-096265-B-I00 and PID2019-104141GB-I00.
[2] Research is supported by Spanish MINECO under grants PID2019-104141GB-I00 and VA169P20.
[3] Research is supported by Spanish MCINYU under grant RTI2018-093521-B-C31 and by the European Union's Horizon 2020 research and innovation program under the Marie Sklodowska-Curie Actions, grant agreement 872442-ARIA.

https://doi.org/10.1016/j.cma.2022.115866

We consider the Navier–Stokes equations

$$\begin{aligned} \partial_t \boldsymbol{u} - \nu \Delta \boldsymbol{u} + (\boldsymbol{u}\cdot\nabla)\boldsymbol{u} + \nabla p &= \boldsymbol{f} && \text{in } (0,T]\times\Omega, \\ \nabla\cdot\boldsymbol{u} &= 0 && \text{in } (0,T]\times\Omega, \end{aligned} \tag{1}$$

in a bounded domain $\Omega \subset \mathbb{R}^d$, $d \in \{2,3\}$ with initial condition $\boldsymbol{u}(0) = \boldsymbol{u}^0$. In (1), $\boldsymbol{u}$ is the velocity field, p the kinematic pressure, $\nu > 0$ the kinematic viscosity coefficient, and $\boldsymbol{f}$ represents the accelerations due to external body forces acting on the fluid. The Navier–Stokes equations (1) must be complemented with boundary conditions. For simplicity, we only consider homogeneous Dirichlet boundary conditions $\boldsymbol{u} = \boldsymbol{0}$ on $\partial\Omega$.

In [1] we can find a definition of FOM–ROM consistency. A ROM is said FOM consistent if it uses the same computational model and numerical discretization as the FOM. As stated in [1]: the theoretical investigation of the FOM–ROM consistency is scarce and investigating the FOM–ROM consistency both computationally and theoretically is an important research direction in reduced order modeling. As in [1], in the present paper we study the consistency related to the nonlinear term. In practical simulations one can apply some given software to compute the snapshots. It could then be the case that a different discretization is used for the discretization of the nonlinear term in the FOM method and the POD method (the last one being typically implemented by means of a hand-made code instead of an existing one). Our aim in this paper is to study the influence of the use of different discretizations for the nonlinear terms on the final error bounds of the POD method.

In [2] POD stabilized methods for the Navier–Stokes equations were considered and analyzed for a case in which the snapshots are based on a non inf–sup stable method and a case in which the snapshots are based on an inf–sup stable method. In the present paper, we consider the second case. Our snapshots are based on an inf–sup stable method and, as in [2], we add grad–div stabilization to both the FOM and the POD methods. We analyze the case in which different discretizations are applied for the nonlinear term. Adding grad–div stabilization we are able to prove error bounds for the method with constants that do not depend explicitly on inverse powers of the viscosity, although, as usual, may depend on it through the norms of the theoretical solution. In the last section, devoted to numerical experiments, we also study the use of different values for the grad–div parameter in the FOM and ROM models. We conclude that it is advisable to use the same values for the grad–div parameter in both models.

In the recent paper [1] we have found an study of the consistency of the nonlinear discretization in FOM and POD methods. In this reference no stabilization is included neither in the FOM nor in the POD method. The authors of [1] conclude that the use of different discretizations in the nonlinear term yields additional terms that prevent the POD method from recovering the FOM accuracy. In the present paper, we prove, in agreement with the results in [1], that there are some additional terms in the error bound of the final POD method coming from the use of different discretizations in the nonlinear terms. We prove that the additional terms have the size of the L^2 error in the velocity and the L^2 error of the divergence of the velocity of the FOM method. This holds both for the methods with grad–div stabilization and also for the plain methods considered in [1]. We then conclude that the extra error term coming from using different discretization for the nonlinear terms in the FOM and POD methods leads in general to a less accurate method although in some examples the extra error is still small and the non consistent FOM–ROM method could be used in practice.

Following [1], we analyzed a concrete case in which the so called divergence or skew-symmetric form of the nonlinear term (commonly used in practice) is used for the FOM method and the EMAC form, see [3], is applied for the POD method. The error analysis for any other combination of discretizations of the nonlinear terms with analogous properties could be carried out in a similar way. The EMAC formulation was designed to conserve energy, momentum and angular momentum. Considering a continuous in time method it is easy to see, as we prove in Section 4, that the effect of grad–div stabilization in a method with EMAC form for the nonlinear term is a lost of kinetic energy. The method maintains however the conservation of the momentum and angular momentum. In practice, as stated in [4], a fully version of a method with EMAC form for the nonlinear term is applied. In [4] it is proved that using Newton method for the nonlinear term is the option from which more quantities are still conserved, although the conservation of the kinetic energy is lost. In this sense, adding grad–div stabilization incurs in the same phenomena so that it seems not to be a hard problem since either kinetic energy or any other properties will be lost with the EMAC formulation in the fully discrete case.

The outline of the paper is as follows. In Section 2 we introduce some notation. In Section 3 we state some preliminaries concerning the POD method. Section 4 is devoted to the error analysis in which one considers different discretizations for the nonlinear term in the FOM and POD methods. In Section 5 we present some numerical experiments. We end the paper with some conclusions.

2. Preliminaries and notation

The following Sobolev embeddings [5] will be used in the analysis: For $q \in [1, \infty)$, there exists a constant $C = C(\Omega, q)$ such that

$$\|v\|_{L^{q'}} \le C\|v\|_{W^{s,q}}, \qquad \frac{1}{q'} \ge \frac{1}{q} - \frac{s}{d} > 0, \quad q < \infty, \quad v \in W^{s,q}(\Omega)^d. \tag{2}$$

The following inequality can be found in [6, Remark 3.35]

$$\|\nabla \cdot \boldsymbol{v}\|_0 \le \|\nabla \boldsymbol{v}\|_0, \quad \boldsymbol{v} \in H_0^1(\Omega)^d, \tag{3}$$

where, here and in the sequel, we use the notation $\|\cdot\|_j$ for $\|\cdot\|_{W^{j,2}} = \|\cdot\|_{H^j}$. Let us denote by $Q = L_0^2(\Omega) = \left\{q \in L^2(\Omega) \mid (q, 1) = 0\right\}$. Let $\mathcal{T}_h = (\tau_j^h, \phi_j^h)_{j \in J_h}$, $h > 0$ be a family of partitions of $\overline{\Omega}$, where h denotes the maximum diameter of the elements $\tau_j^h \in \mathcal{T}_h$, and ϕ_j^h are the mappings from the reference simplex τ_0 onto τ_j^h. We shall assume that the partitions are shape-regular and quasi-uniform. We define the following finite element spaces

$$\begin{aligned} Y_h^l &= \left\{v_h \in C^0(\overline{\Omega}) \mid v_{h|_K} \in \mathbb{P}_l(K), \quad \forall K \in \mathcal{T}_h\right\}, \ l \ge 1, \\ \boldsymbol{Y}_h^l &= (Y_h^l)^d, \quad \boldsymbol{X}_h^l = \boldsymbol{Y}_h^l \cap H_0^1(\Omega)^d, \\ Q_h^l &= Y_h^l \cap L_0^2(\Omega). \end{aligned}$$

$$\boldsymbol{V}_{h,l} = \boldsymbol{X}_h^l \cap \left\{\boldsymbol{\chi}_h \in H_0^1(\Omega)^d \mid (q_h, \nabla \cdot \boldsymbol{\chi}_h) = 0 \quad \forall q_h \in Q_h^{l-1}\right\}, \quad l \ge 2. \tag{4}$$

If the family of meshes is quasi-uniform then the following inverse inequality holds for each $\boldsymbol{v}_h \in Y_h^l$, see e.g., [7, Theorem 3.2.6],

$$\|\boldsymbol{v}_h\|_{W^{m,p}(K)} \le c_{\text{inv}} h_K^{n-m-d\left(\frac{1}{q}-\frac{1}{p}\right)} \|\boldsymbol{v}_h\|_{W^{n,q}(K)}, \tag{5}$$

where $0 \le n \le m \le 1$, $1 \le q \le p \le \infty$, and h_K is the diameter of $K \in \mathcal{T}_h$. Let $l \ge 2$, we consider the MFE pair known as Hood–Taylor elements [8,9] $(\boldsymbol{X}_h^l, Q_h^{l-1})$.

For these elements a uniform inf–sup condition is satisfied (see [8]), that is, there exists a constant $\beta_{\text{is}} > 0$ independent of the mesh size h such that

$$\inf_{q_h \in Q_h^{l-1}} \sup_{\boldsymbol{v}_h \in \boldsymbol{X}_h^l} \frac{(q_h, \nabla \cdot \boldsymbol{v}_h)}{\|\boldsymbol{v}_h\|_1 \|q_h\|_{L^2/\mathbb{R}}} \ge \beta_{\text{is}}. \tag{6}$$

We will denote by P_{Q_h} the L^2 orthogonal projection onto Q_h^{l-1}. The following bound holds

$$\|q - P_{Q_h} q\|_0 \le C h^l \|q\|_l, \quad \forall q \in H^l(\Omega). \tag{7}$$

As a direct method, as in [2, Section 5], we consider a Galerkin method with grad–div stabilization and for simplicity in the analysis we consider the implicit Euler method in time. Let us fix $T > 0$ and $M > 0$ and take $\Delta t = T/M$. The method reads as follows: given $\boldsymbol{u}_h^0 \approx \boldsymbol{u}_0$ find $(\boldsymbol{u}_h^n, p_h^n) \in \boldsymbol{X}_h^l \times Q_h^{l-1}$ for $n \ge 1$ such that

$$\begin{aligned} &\left(\frac{\boldsymbol{u}_h^n - \boldsymbol{u}_h^{n-1}}{\Delta t}, \boldsymbol{v}_h\right) + \nu(\nabla \boldsymbol{u}_h^n, \nabla \boldsymbol{v}_h) + b_h(\boldsymbol{u}_h^n, \boldsymbol{u}_h^n, \boldsymbol{v}_h) - (p_h^n, \nabla \cdot \boldsymbol{v}_h) \\ &\quad + \mu(\nabla \cdot \boldsymbol{u}_h^n, \nabla \cdot \boldsymbol{v}_h) = (\boldsymbol{f}^n, \boldsymbol{v}_h) \quad \forall \boldsymbol{v}_h \in \boldsymbol{X}_h^l, \\ &(\nabla \cdot \boldsymbol{u}_h^n, q_h) = 0 \quad \forall q_h \in Q_h^{l-1}, \end{aligned} \tag{8}$$

where μ is the positive grad–div stabilization parameter.

For the discretization of the nonlinear term we consider the following form, the so called divergence or skew-symmetric form,

$$b_h(\boldsymbol{u}, \boldsymbol{v}, \boldsymbol{w}) = ((\boldsymbol{u} \cdot \nabla \boldsymbol{v}), \boldsymbol{w}) + \frac{1}{2}((\nabla \cdot \boldsymbol{u})\boldsymbol{v}, \boldsymbol{w}). \tag{9}$$

It is well-known that considering the discrete divergence-free space $\boldsymbol{V}_{h,l}$ we can remove the pressure from (8) since $\boldsymbol{u}_h^n \in \boldsymbol{V}_{h,l}$ satisfies for $n \geq 1$

$$\left(\frac{\boldsymbol{u}_h^n - \boldsymbol{u}_h^{n-1}}{\Delta t}, \boldsymbol{v}_h\right) + \nu(\nabla \boldsymbol{u}_h^n, \nabla \boldsymbol{v}_h) + b_h(\boldsymbol{u}_h^n, \boldsymbol{u}_h^n, \boldsymbol{v}_h) + \mu(\nabla \cdot \boldsymbol{u}_h^n, \nabla \cdot \boldsymbol{v}_h) = (\boldsymbol{f}^n, \boldsymbol{v}_h), \quad \forall \boldsymbol{v}_h \in \boldsymbol{V}_{h,l}. \tag{10}$$

For this method the following bound holds, see [10]

$$\|\boldsymbol{u}^n - \boldsymbol{u}_h^n\|_0 + \left(\mu \sum_{j=1}^{M} \Delta t \|\nabla \cdot (\boldsymbol{u}^n - \boldsymbol{u}_h^n)\|_0^2\right)^{1/2} \leq C(\boldsymbol{u}, p, l+1)\left(h^l + \Delta t\right), \tag{11}$$

for $1 \leq n \leq M$, where the constant $C(\boldsymbol{u}, p, l+1)$ depends on $\|\boldsymbol{u}\|_{L^\infty(H^{l+1})}$, $\left(\int_0^T \|\boldsymbol{u}_t\|_l^2\right)^{1/2}$, $\left(\int_0^T \|\boldsymbol{u}_{tt}\|_0^2\right)^{1/2}$ and $\|p\|_{L^\infty(H^l)}$ but does not depend explicitly on inverse powers of ν.

For the plain Galerkin method the following bound holds where the error constants depend explicitly on inverse powers of ν

$$\|\boldsymbol{u}^n - \boldsymbol{u}_h^n\|_0 + h\|\nabla(\boldsymbol{u}^n - \boldsymbol{u}_h^n)\|_0 \leq C(\boldsymbol{u}, p, \nu^{-1}, l+1)\left(h^{l+1} + \Delta t\right). \tag{12}$$

3. Proper orthogonal decomposition

We will consider a proper orthogonal decomposition (POD) method. As for the FOM we fix $T > 0$ and $M > 0$ and take $\Delta t = T/M$. We consider the following space

$$\boldsymbol{U} = \langle \boldsymbol{u}_h^1, \ldots, \boldsymbol{u}_h^M \rangle,$$

where $\boldsymbol{u}_h^j = \boldsymbol{u}_h(\cdot, t_j)$. Let d_v be the dimension of the space $\boldsymbol{U}$.

Let K_v be the correlation matrix corresponding to the snapshots $K_v = ((k_{i,j}^v)) \in \mathbb{R}^{M\times M}$, where

$$k_{i,j}^v = \frac{1}{M}(\boldsymbol{u}_h^i, \boldsymbol{u}_h^j),$$

and $(\cdot,\cdot)$ is the inner product in $L^2(\Omega)^d$. Following [11] we denote by $\lambda_1 \geq \lambda_2, \ldots \geq \lambda_{d_v} > 0$ the positive eigenvalues of K_v and by $\boldsymbol{v}_1, \ldots, \boldsymbol{v}_{d_v} \in \mathbb{R}^M$ the associated eigenvectors. Then, the (orthonormal) POD bases are given by

$$\boldsymbol{\varphi}_k = \frac{1}{\sqrt{M}} \frac{1}{\sqrt{\lambda_k}} \sum_{j=1}^{M} v_k^j \boldsymbol{u}_h(\cdot, t_j), \tag{13}$$

where v_k^j is the jth component of the eigenvector $\boldsymbol{v}_k$ and the following error formulas hold, see [11, Proposition 1]

$$\frac{1}{M}\sum_{j=0}^{M} \|\boldsymbol{u}_h^j - \sum_{k=1}^{r} (\boldsymbol{u}_h^j, \boldsymbol{\varphi}_k)\boldsymbol{\varphi}_k\|_0^2 \;\leq\; \sum_{k=r+1}^{d_v} \lambda_k. \tag{14}$$

We will denote by S^v the stiffness matrix for the POD basis: $S^v = ((s_{i,j}^v)) \in \mathbb{R}^{d_v \times d_v}$, $s_{i,j}^v = (\nabla \boldsymbol{\varphi}_i, \nabla \boldsymbol{\varphi}_j)$. In that case, for any $\boldsymbol{v} \in \boldsymbol{U}$, the following inverse inequality holds, see [11, Lemma 2]

$$\|\nabla \boldsymbol{v}\|_0 \leq \sqrt{\|S^v\|_2}\|\boldsymbol{v}\|_0. \tag{15}$$

In the sequel we will denote by

$$\boldsymbol{U}^r = \langle \boldsymbol{\varphi}_1, \boldsymbol{\varphi}_2, \ldots, \boldsymbol{\varphi}_r \rangle,$$

and by P_r^v, the L^2-orthogonal projection onto $\boldsymbol{U}^r$.

3.1. A priori bounds for the orthogonal projection onto $\boldsymbol{U}^r$

In [2, Section 3.1] some a priori bounds for the FOM and for the orthogonal projection were obtained assuming for the solution of (1) the same regularity needed to prove (11). For $0 \le j \le M$ the following bound holds (see [2, (31), (35)])

$$\|\boldsymbol{u}_h^j\|_\infty \le C_{\boldsymbol{u},\mathrm{inf}} \tag{16}$$

$$\|\nabla \boldsymbol{u}_h^j\|_{L^{2d/(d-1)}} \le C_{\boldsymbol{u},\mathrm{ld}}. \tag{17}$$

For $1 \le j \le M$ the following bounds hold (see [2, (39), (40), (41)])

$$\|P_r^v \boldsymbol{u}_h^j\|_\infty \le C_{\mathrm{inf}}, \tag{18}$$

$$\|\nabla P_r^v \boldsymbol{u}_h^j\|_\infty \le C_{1,\mathrm{inf}}, \tag{19}$$

$$\|\nabla P_r^v \boldsymbol{u}^j\|_{L^{2d/(d-1)}} \le C_{\mathrm{ld}}. \tag{20}$$

4. The POD method

We now consider the grad–div POD model. As for the full order model, for simplicity in the error analysis, we also use the implicit Euler method as time integrator. Taking an initial approximation $\boldsymbol{u}_r^0 \in \boldsymbol{U}^r$, for $n \ge 1$, find $\boldsymbol{u}_r^n \in \boldsymbol{U}^r$ such that

$$\left(\frac{\boldsymbol{u}_r^n - \boldsymbol{u}_r^{n-1}}{\Delta t}, \boldsymbol{\varphi}\right) + \nu(\nabla \boldsymbol{u}_r^n, \nabla \boldsymbol{\varphi}) + b_{pod}(\boldsymbol{u}_r^n, \boldsymbol{u}_r^n, \boldsymbol{\varphi}) + \mu(\nabla \cdot \boldsymbol{u}_r^n, \nabla \cdot \boldsymbol{\varphi}) = (\boldsymbol{f}^n, \boldsymbol{\varphi}), \quad \forall \boldsymbol{\varphi} \in \boldsymbol{U}^r, \tag{21}$$

where we observe that $\boldsymbol{U}^r \subset \boldsymbol{V}_{h,l}$ so that there is no pressure approximation in (21). For the discretization of the nonlinear term we consider the EMAC form

$$b_{pod}(\boldsymbol{u}, \boldsymbol{v}, \boldsymbol{w}) = (2D(\boldsymbol{u})\boldsymbol{v}, \boldsymbol{w}) + ((\nabla \cdot \boldsymbol{u})\boldsymbol{v}, \boldsymbol{w}), \tag{22}$$

where the deformation tensor is

$$D(\boldsymbol{u}) = \frac{1}{2}\left(\nabla \boldsymbol{u} + (\nabla \boldsymbol{u})^T\right),$$

and the second term in (22) is added to ensure the property

$$b_{pod}(\boldsymbol{v}, \boldsymbol{v}, \boldsymbol{v}) = 0. \tag{23}$$

The EMAC form is based on the identity

$$(\boldsymbol{u} \cdot \nabla)\boldsymbol{u} = 2D(\boldsymbol{u})\boldsymbol{u} - \frac{1}{2}\nabla|\boldsymbol{u}|^2. \tag{24}$$

From (24) it can be observed that the EMAC form of the nonlinear term implies a modification of the pressure, i.e., in a velocity–pressure formulation of a method with the EMAC form for the nonlinear term the pressure approximation converges to $p - \frac{1}{2}|\boldsymbol{u}|^2$ instead of to the original pressure p in (1).

Considering for simplicity the continuous in time case, i.e., the method:

$$\left(\boldsymbol{u}_{r,t}, \boldsymbol{\varphi}\right) + \nu(\nabla \boldsymbol{u}_r, \nabla \boldsymbol{\varphi}) + b_{pod}(\boldsymbol{u}_r, \boldsymbol{u}_r, \boldsymbol{\varphi}) + \mu(\nabla \cdot \boldsymbol{u}_r, \nabla \cdot \boldsymbol{\varphi}) = (\boldsymbol{f}, \boldsymbol{\varphi}),$$

taking $\boldsymbol{\varphi} = \boldsymbol{u}_r$ and assuming as in [3,4], $\boldsymbol{f} = 0$ and $\nu = 0$ one gets applying (23)

$$\frac{d}{dt}\|\boldsymbol{u}_r\|_0^2 = -\mu\|\nabla \cdot \boldsymbol{u}_r\|_0^2. \tag{25}$$

This means that the grad–div stabilization produces a lost in the kinetic energy. As stated in the introduction, considering a fully discrete method with Newton discretization for the nonlinear term one has also the effect of a lost of kinetic energy, see [4]. On the other hand, it is easy to prove that the grad–div term has no negative effect in the conservation of linear and angular momentum so that both are still conserved. To prove this, one can argue as in [12, Theorem 3.3] and observe that the test functions used to achieve the conservation of linear and angular momentum have divergence zero so that the grad–div term does not affect the proof.

4.1. Error analysis of the method

Denoting by

$$\boldsymbol{\eta}_h^n = P_r^v \boldsymbol{u}_h^n - \boldsymbol{u}_h^n,$$

it is easy to get

$$\begin{aligned}
&\left(\frac{P_r^v \boldsymbol{u}_h^n - P_r^v \boldsymbol{u}_h^{n-1}}{\Delta t}, \boldsymbol{\varphi}\right) + \nu(\nabla P_r^v \boldsymbol{u}_h^n, \nabla\boldsymbol{\varphi}) + b_h(P_r^v \boldsymbol{u}_h^n, P_r^v \boldsymbol{u}_h^n, \boldsymbol{\varphi}) \\
&\quad + \mu(\nabla \cdot P_r^v \boldsymbol{u}_h^n, \nabla\cdot\boldsymbol{\varphi}) \\
&= (\boldsymbol{f}^n, \boldsymbol{\varphi}) + \nu(\nabla\boldsymbol{\eta}_h^n, \nabla\boldsymbol{\varphi}) + \mu(\nabla\cdot\boldsymbol{\eta}_h^n, \nabla\cdot\boldsymbol{\varphi}) \\
&\quad + b_h(P_r^v \boldsymbol{u}_h^n, P_r^v \boldsymbol{u}_h^n, \boldsymbol{\varphi}) - b_h(\boldsymbol{u}_h^n, \boldsymbol{u}_h^n, \boldsymbol{\varphi}), \quad \forall \boldsymbol{\varphi} \in \boldsymbol{U}^r.
\end{aligned} \tag{26}$$

Subtracting (26) from (21) and denoting by

$$\boldsymbol{e}_r^n = \boldsymbol{u}_r^n - P_r^v \boldsymbol{u}_h^n$$

we get $\forall \boldsymbol{\varphi} \in \mathcal{U}^r$

$$\begin{aligned}
&\left(\frac{\boldsymbol{e}_r^n - \boldsymbol{e}_r^{n-1}}{\Delta t}, \boldsymbol{\varphi}\right) + \nu(\nabla\boldsymbol{e}_r^n, \nabla\boldsymbol{\varphi}) + \mu(\nabla\cdot\boldsymbol{e}_r^n, \nabla\cdot\boldsymbol{\varphi}) \\
&= \left(b_h(\boldsymbol{u}_h^n, \boldsymbol{u}_h^n, \boldsymbol{\varphi}) - b_{pod}(\boldsymbol{u}_r^n, \boldsymbol{u}_r^n, \boldsymbol{\varphi})\right) - \nu(\nabla\boldsymbol{\eta}_h^n, \nabla\boldsymbol{\varphi}) - \mu(\nabla\cdot\boldsymbol{\eta}_h^n, \nabla\cdot\boldsymbol{\varphi}).
\end{aligned} \tag{27}$$

Taking $\boldsymbol{\varphi} = \boldsymbol{e}_r^n$ we obtain

$$\begin{aligned}
&\frac{1}{2\Delta t}\left(\|\boldsymbol{e}_r^n\|_0^2 - \|\boldsymbol{e}_r^{n-1}\|_0^2\right) + \nu\|\nabla\boldsymbol{e}_r^n\|_0^2 + \mu\|\nabla\cdot\boldsymbol{e}_r^n\|_0^2 \\
&\quad \le \left(b_h(\boldsymbol{u}_h^n, \boldsymbol{u}_h^n, \boldsymbol{e}_r^n) - b_{pod}(\boldsymbol{u}_r^n, \boldsymbol{u}_r^n, \boldsymbol{e}_r^n)\right) - \nu(\nabla\boldsymbol{\eta}_h^n, \nabla\boldsymbol{e}_r^n) - \mu(\nabla\cdot\boldsymbol{\eta}_h^n, \nabla\cdot\boldsymbol{e}_r^n) \\
&\quad = I + II + III.
\end{aligned} \tag{28}$$

We will bound the first term on the right-hand side above. Arguing as in [1] we get

$$\begin{aligned}
|I| \le\ & \left|b_{pod}(\boldsymbol{u}_h^n, \boldsymbol{u}_h^n, \boldsymbol{e}_r^n) - b_{pod}(\boldsymbol{u}_r^n, \boldsymbol{u}_r^n, \boldsymbol{e}_r^n)\right| \\
&+ \left|b_h(\boldsymbol{u}_h^n, \boldsymbol{u}_h^n, \boldsymbol{e}_r^n) - b_{pod}(\boldsymbol{u}_h^n, \boldsymbol{u}_h^n, \boldsymbol{e}_r^n)\right|.
\end{aligned} \tag{29}$$

To bound the first term on the right-hand side of (29) we argue as in [13] (see also [14]). We first observe that

$$\begin{aligned}
&b_{pod}(\boldsymbol{u}_h^n, \boldsymbol{u}_h^n, \boldsymbol{e}_r^n) - b_{pod}(\boldsymbol{u}_r^n, \boldsymbol{u}_r^n, \boldsymbol{e}_r^n) = b_{pod}(-\boldsymbol{\eta}_h^n, \boldsymbol{u}_h^n, \boldsymbol{e}_r^n) \\
&\quad + b_{pod}(P_r^v \boldsymbol{u}_h^n, -\boldsymbol{\eta}_h^n, \boldsymbol{e}_r^n) - b_{pod}(P_r^v \boldsymbol{u}_h^n, \boldsymbol{e}_r^n, \boldsymbol{e}_r^n) \\
&\quad - b_{pod}(\boldsymbol{e}_r^n, P_r^v \boldsymbol{u}_h^n, \boldsymbol{e}_r^n) - b_{pod}(\boldsymbol{e}_r^n, \boldsymbol{e}_r^n, \boldsymbol{e}_r^n).
\end{aligned} \tag{30}$$

The last term on the right-hand side of (30) vanishes due to the property (23). The expression of the fourth one is

$$b_{pod}(\boldsymbol{e}_r^n, P_r^v \boldsymbol{u}_h^n, \boldsymbol{e}_r^n) = ((P_r^v \boldsymbol{u}_h^n \cdot \nabla)\boldsymbol{e}_r^n, \boldsymbol{e}_r^n) + ((\boldsymbol{e}_r^n \cdot \nabla)\boldsymbol{e}_r^n, P_r^v \boldsymbol{u}_h^n) + ((\nabla\cdot\boldsymbol{e}_r^n)\boldsymbol{e}_r^n, P_r^v \boldsymbol{u}_h^n).$$

Integration by parts reveals that the first term on the right-hand side above equals $-\frac{1}{2}((\nabla\cdot P_r^v \boldsymbol{u}_h^n)\boldsymbol{e}_r^n, \boldsymbol{e}_r^n)$, whilst the other two equal $-((\boldsymbol{e}_r^n \cdot \nabla)P_r^v \boldsymbol{u}_h^n, \boldsymbol{e}_r^n)$, so that

$$b_{pod}(\boldsymbol{e}_r^n, P_r^v \boldsymbol{u}_h^n, \boldsymbol{e}_r^n) = -\frac{1}{2}((\nabla\cdot P_r^v \boldsymbol{u}_h^n)\boldsymbol{e}_r^n, \boldsymbol{e}_r^n) - ((\boldsymbol{e}_r^n \cdot \nabla)P_r^v \boldsymbol{u}_h^n, \boldsymbol{e}_r^n).$$

Since the third term on the right-hand side of (30) is

$$b_{pod}(P_r^v \boldsymbol{u}_h^n, \boldsymbol{e}_r^n, \boldsymbol{e}_r^n) = 2((\boldsymbol{e}_r^n \cdot \nabla)P_r^v \boldsymbol{u}_h^n, \boldsymbol{e}_r^n) + ((\nabla\cdot P_r^v \boldsymbol{u}_h^n)\boldsymbol{e}_r^n, \boldsymbol{e}_r^n),$$

we see that the last three terms on the right-hand side of (30) add to $-((\boldsymbol{e}_r^n\cdot\nabla)P_r^v\boldsymbol{u}_h^n,\boldsymbol{e}_r^n)-\frac{1}{2}((\nabla\cdot P_r^v\boldsymbol{u}_h^n)\boldsymbol{e}_r^n,\boldsymbol{e}_r^n)$, so that (30) can be written as

$$b_{pod}(\boldsymbol{u}_h^n,\boldsymbol{u}_h^n,\boldsymbol{e}_r^n)-b_{pod}(\boldsymbol{u}_r^n,\boldsymbol{u}_r^n,\boldsymbol{e}_r^n)=b_{pod}(-\boldsymbol{\eta}_h^n,\boldsymbol{u}_h^n,\boldsymbol{e}_r^n) \tag{31}$$
$$+b_{pod}(P_r^v\boldsymbol{u}_h^n,-\boldsymbol{\eta}_h^n,\boldsymbol{e}_r^n)-\frac{1}{2}((\nabla\cdot P_r^v\boldsymbol{u}_h^n)\boldsymbol{e}_r^n,\boldsymbol{e}_r^n)-(D(P_r^v\boldsymbol{u}_h^n)\boldsymbol{e}_r^n,\boldsymbol{e}_r^n).$$

For the first term on the right-hand side of (31), applying (16), we obtain

$$b_{pod}(-\boldsymbol{\eta}_h^n,\boldsymbol{u}_h^n,\boldsymbol{e}_r^n)\le C\|\boldsymbol{\eta}_h^n\|_1\|\boldsymbol{u}_h^n\|_\infty\|\boldsymbol{e}_r^n\|_0\le CC_{\boldsymbol{u},\inf}\|\boldsymbol{\eta}_h^n\|_1\|\boldsymbol{e}_r^n\|_0. \tag{32}$$

Applying Hölder's inequality, (19) and Sobolev embedding (2) we get for the second term on the right-hand side of (31)

$$\begin{aligned}b_{pod}(P_r^v\boldsymbol{u}_h^n,-\boldsymbol{\eta}_h^n,\boldsymbol{e}_r^n)&\le 2\|D(P_r^v\boldsymbol{u}_h^n)\|_{L^{2d/(d-1)}}\|\boldsymbol{\eta}_h^n\|_{L^{2d}}\|\boldsymbol{e}_r^n\|_0\\&\quad+\|\nabla\cdot P_r^v\boldsymbol{u}_h^n\|_{L^{2d/(d-1)}}\|\boldsymbol{\eta}_h^n\|_{L^{2d}}\|\boldsymbol{e}_r^n\|_0\\&\le C\|\nabla P_r^v\boldsymbol{u}_h^n\|_{L^{2d/(d-1)}}\|\boldsymbol{\eta}_h^n\|_{L^{2d}}\|\boldsymbol{e}_r^n\|_0\\&\le CC_{\mathrm{ld}}\|\boldsymbol{\eta}_h^n\|_1\|\boldsymbol{e}_r^n\|_0.\end{aligned} \tag{33}$$

Finally, for the last two terms on the right-hand side of (31), applying (19), we get

$$-\frac{1}{2}((\nabla\cdot P_r^v\boldsymbol{u}_h^n)\boldsymbol{e}_r^n,\boldsymbol{e}_r^n)-(D(P_r^v\boldsymbol{u}_h^n)\boldsymbol{e}_r^n,\boldsymbol{e}_r^n)\le CC_{1,\inf}\|\boldsymbol{e}_r^n\|_0^2. \tag{34}$$

From (31), (32), (33) and (34) and Poincaré inequality we finally reach

$$\begin{aligned}&|b_{pod}(\boldsymbol{u}_h^n,\boldsymbol{u}_h^n,\boldsymbol{e}_r^n)-b_{pod}(\boldsymbol{u}_r^n,\boldsymbol{u}_r^n,\boldsymbol{e}_r^n)|\\&\quad\le(1+CC_{1,\inf})\|\boldsymbol{e}_r^n\|_0^2+C(C_{\boldsymbol{u},\inf}^2+C_{\mathrm{ld}}^2)\|\nabla\boldsymbol{\eta}_h^n\|_0^2.\end{aligned} \tag{35}$$

For the second term on the right-hand side of (29), we recall that

$$b_h(\boldsymbol{u}_h^n,\boldsymbol{u}_h^n,\boldsymbol{e}_r^n)=(\boldsymbol{u}_h^n\cdot\nabla\boldsymbol{u}_h^n,\boldsymbol{e}_r^n)+\frac{1}{2}((\nabla\cdot\boldsymbol{u}_h^n)\boldsymbol{u}_h^n,\boldsymbol{e}_r^n).$$
$$b_{pod}(\boldsymbol{u}_h^n,\boldsymbol{u}_h^n,\boldsymbol{e}_r^n)=(\boldsymbol{u}_h^n\cdot\nabla\boldsymbol{u}_h^n,\boldsymbol{e}_r^n)+(\boldsymbol{e}_r^n\cdot\nabla\boldsymbol{u}_h^n,\boldsymbol{u}_h^n)+((\nabla\cdot\boldsymbol{u}_h^n)\boldsymbol{u}_h^n,\boldsymbol{e}_r^n).$$

We notice that both $b_h(\boldsymbol{u}_h^n,\boldsymbol{u}_h^n,\boldsymbol{e}_r^n)$ and $b_{pod}(\boldsymbol{u}_h^n,\boldsymbol{u}_h^n,\boldsymbol{e}_r^n)$ share the term $(\boldsymbol{u}_h^n\cdot\nabla\boldsymbol{u}_h^n,\boldsymbol{e}_r^n)$, and both also have the term $((\nabla\cdot\boldsymbol{u}_h^n)\boldsymbol{u}_h^n,\boldsymbol{e}_r^n)$ but with a factor $1/2$ in the second one, so that we have

$$b_h(\boldsymbol{u}_h^n,\boldsymbol{u}_h^n,\boldsymbol{e}_r^n)-b_{pod}(\boldsymbol{u}_h^n,\boldsymbol{u}_h^n,\boldsymbol{e}_r^n)=-(\boldsymbol{e}_r^n\cdot\nabla\boldsymbol{u}_h^n,\boldsymbol{u}_h^n)-\frac{1}{2}((\nabla\cdot\boldsymbol{u}_h^n)\boldsymbol{u}_h^n,\boldsymbol{e}_r^n)$$

Now, integrating by parts the first term on the right-hand side above we have

$$b_h(\boldsymbol{u}_h^n,\boldsymbol{u}_h^n,\boldsymbol{e}_r^n)-b_{pod}(\boldsymbol{u}_h^n,\boldsymbol{u}_h^n,\boldsymbol{e}_r^n)=\frac{1}{2}(|\boldsymbol{u}_h^n|^2,\nabla\cdot\boldsymbol{e}_r^n)-\frac{1}{2}((\nabla\cdot\boldsymbol{u}_h^n)\boldsymbol{u}_h^n,\boldsymbol{e}_r^n),$$

and, since $\nabla\cdot\boldsymbol{u}=0$, we can write

$$b_h(\boldsymbol{u}_h^n,\boldsymbol{u}_h^n,\boldsymbol{e}_r^n)-b_{pod}(\boldsymbol{u}_h^n,\boldsymbol{u}_h^n,\boldsymbol{e}_r^n)=\frac{1}{2}(|\boldsymbol{u}_h^n|^2,\nabla\cdot\boldsymbol{e}_r^n)+\frac{1}{2}((\nabla\cdot(\boldsymbol{u}^n-\boldsymbol{u}_h^n))\boldsymbol{u}_h^n,\boldsymbol{e}_r^n), \tag{36}$$

For the second term on the right-hand side of (36) we have

$$\begin{aligned}\frac{1}{2}((\nabla\cdot(\boldsymbol{u}^n-\boldsymbol{u}_h^n))\boldsymbol{u}_h^n,\boldsymbol{e}_r^n)&\le\frac{1}{2}\|\boldsymbol{u}_h^n\|_\infty\|\nabla\cdot(\boldsymbol{u}_h^n-\boldsymbol{u}^n)\|_0\|\boldsymbol{e}_r^n\|_0\\&\le C_{\boldsymbol{u},\inf}^2\frac{\mu}{4}\|\nabla\cdot(\boldsymbol{u}_h^n-\boldsymbol{u}^n)\|_0^2+\frac{1}{4\mu}\|\boldsymbol{e}_r^n\|_0^2,\end{aligned} \tag{37}$$

For the first term on the right-hand side of (36), we have

$$\begin{aligned}
&\frac{1}{2}(|\boldsymbol{u}_h^n|^2, \nabla\cdot\boldsymbol{e}_r^n)| \le \frac{1}{2}(|\boldsymbol{u}_h^n|^2 - |\boldsymbol{u}^n|^2, \nabla\cdot\boldsymbol{e}_r^n)| + \frac{1}{2}|(|\boldsymbol{u}^n|^2, \nabla\cdot\boldsymbol{e}_r^n)| \\
&= \frac{1}{2}|(|\boldsymbol{u}_h^n|^2 - |\boldsymbol{u}^n|^2, \nabla\cdot\boldsymbol{e}_r^n)| + \frac{1}{2}|((I-P_{Q_h})|\boldsymbol{u}^n|^2, \nabla\cdot\boldsymbol{e}_r^n)| \\
&\le \frac{1}{2}\|\boldsymbol{u}^n + \boldsymbol{u}_h^n\|_\infty \|\boldsymbol{u}^n - \boldsymbol{u}_h^n\|_0 \|\nabla\cdot\boldsymbol{e}_r^n\|_0 + \frac{1}{2}\|(I-P_{Q_h})|\boldsymbol{u}^n|^2\|_0 \|\nabla\cdot\boldsymbol{e}_r^n\|_0.
\end{aligned} \tag{38}$$

Then, applying (16)

$$\begin{aligned}
&\frac{1}{2}|(|\boldsymbol{u}_h^n|^2, \nabla\cdot\boldsymbol{e}_r^n)| \le \frac{1}{2}(\|\boldsymbol{u}^n\|_\infty + C_{\boldsymbol{u},\mathrm{inf}})\|\boldsymbol{u}^n - \boldsymbol{u}_h^n\|_0 \|\nabla\cdot\boldsymbol{e}_r^n\|_0 \\
&\quad + \frac{1}{2}\|(I-P_{Q_h})|\boldsymbol{u}^n|^2\|_0 \|\nabla\cdot\boldsymbol{e}_r^n\|_0 \le C\mu^{-1}(\|\boldsymbol{u}^n - \boldsymbol{u}_h^n\|_0^2 + \|(I-P_{Q_h})|\boldsymbol{u}^n|^2\|_0^2) \\
&\quad + \frac{\mu}{4}\|\nabla\cdot\boldsymbol{e}_r^n\|_0^2,
\end{aligned} \tag{39}$$

where the generic constant C above depends on $\|\boldsymbol{u}\|_{L^\infty(L^\infty)}$ and $C_{\boldsymbol{u},\mathrm{inf}}$. Inserting (35), (36), (37) and (39) into (29) we get

$$\begin{aligned}
|I| \le &\left(1 + CC_{1,\mathrm{inf}} + \frac{1}{4\mu}\right)\|\boldsymbol{e}_r^n\|_0^2 + \frac{\mu}{4}\|\nabla\cdot\boldsymbol{e}_r^n\|_0^2 \\
&+ C(C_{\boldsymbol{u},\mathrm{inf}}^2 + C_{\mathrm{ld}}^2)\|\nabla\boldsymbol{\eta}_h^n\|_0^2 + C_{\boldsymbol{u},\mathrm{inf}}^2\frac{\mu}{4}\|\nabla\cdot(\boldsymbol{u}_h^n - \boldsymbol{u}^n)\|_0^2 \\
&+ C\mu^{-1}(\|\boldsymbol{u} - \boldsymbol{u}_h\|_0^2 + \|(I-P_{Q_h})|\boldsymbol{u}^n|^2\|_0^2).
\end{aligned}$$

Including into a generic constant C the dependence on $C_{\boldsymbol{u},\mathrm{inf}}$ and C_{ld} of the third and fourth terms above we may write

$$\begin{aligned}
|I| \le &\left(1 + CC_{1,\mathrm{inf}} + \frac{1}{4\mu}\right)\|\boldsymbol{e}_r^n\|_0^2 + \frac{\mu}{4}\|\nabla\cdot\boldsymbol{e}_r^n\|_0^2 \\
&+ C\|\nabla\boldsymbol{\eta}_h^n\|_0^2 + C\mu\|\nabla\cdot(\boldsymbol{u}_h^n - \boldsymbol{u}^n)\|_0^2 \\
&+ C\mu^{-1}(\|\boldsymbol{u} - \boldsymbol{u}_h\|_0^2 + \|(I-P_{Q_h})|\boldsymbol{u}^n|^2\|_0^2).
\end{aligned} \tag{40}$$

We also have

$$|II| \le \frac{\nu}{2}\|\nabla\boldsymbol{\eta}_h^n\|_0^2 + \frac{\nu}{2}\|\nabla\boldsymbol{e}_r^n\|_0^2, \tag{41}$$

and

$$|III| \le \|\nabla\cdot\boldsymbol{\eta}_h^n\|_0^2 + \frac{\mu}{4}\|\nabla\cdot\boldsymbol{e}_r^n\|_0^2. \tag{42}$$

Inserting (40), (41) and (42) into (28) and adding terms we get

$$\begin{aligned}
&\|\boldsymbol{e}_r^n\|_0^2 + \nu\sum_{j=1}^n \Delta t\|\nabla\boldsymbol{e}_r^j\|_0^2 + \mu\sum_{j=1}^n \Delta t\|\nabla\cdot\boldsymbol{e}_r^j\|_0^2 \\
&\le \|\boldsymbol{e}_r^0\|_0^2 + \sum_{j=1}^n \Delta t\left(1 + CC_{1,\mathrm{inf}} + \frac{1}{4\mu}\right)\|\boldsymbol{e}_r^j\|_0^2 + C(\nu+\mu)\sum_{j=1}^n \Delta t\|\nabla\boldsymbol{\eta}_h^j\|_0^2 \\
&\quad + C\mu\sum_{j=1}^n \Delta t\|\nabla\cdot(\boldsymbol{u}_h^j - \boldsymbol{u}^j)\|_0^2 + C\mu^{-1}\sum_{j=1}^n \Delta t\|\boldsymbol{u}_h^j - \boldsymbol{u}^j\|_0^2 \\
&\quad + C\mu^{-1}\sum_{j=1}^n \Delta t\|(I-P_{Q_h})|\boldsymbol{u}^j|^2\|_0^2.
\end{aligned} \tag{43}$$

Assuming

$$\Delta t C_u := \Delta t(1 + CC_{1,\inf} + \frac{1}{4\mu}) \le \frac{1}{2} \tag{44}$$

and applying Gronwall's Lemma [15, Lemma 5.1] and (14), (15), (11) and (7) we obtain

$$\begin{aligned}
&\|\boldsymbol{e}_r^n\|_0^2 + \nu \sum_{j=1}^{n} \Delta t \|\nabla \boldsymbol{e}_r^j\|_0^2 + \mu \sum_{j=1}^{n} \Delta t \|\nabla \cdot \boldsymbol{e}_r^j\|_0^2 \\
&\le e^{2TC_u} \left(\|\boldsymbol{e}_r^0\|_0^2 + CT(\nu+\mu)\|S^v\|_0 \sum_{k=r+1}^{d_v} \lambda_k \right. \\
&\left. + C(1+\mu^{-1}T)C(\boldsymbol{u}, p, l+1)^2 \left(h^{2l} + (\Delta t)^2\right) + C\mu^{-1}h^{2l}T\||\boldsymbol{u}|^2\|_{L^\infty(H^l)} \right).
\end{aligned} \tag{45}$$

Remark 4.1. Let us observe that the error terms in the last line of (45) arise from using different discretization for the nonlinear term in the FOM and the POD methods. We also observe that these errors are of the same size as the error of the FOM method. More precisely, in view of (37) and (38), the extra errors have the size of $\mu\|\nabla\cdot(\boldsymbol{u}_h^n - \boldsymbol{u}^n)\|_0^2$, $\|\boldsymbol{u} - \boldsymbol{u}_h\|_0^2$ and $\|(I - P_{Q_h})|\boldsymbol{u}^n|^2\|_0^2$ times several constants of the same size as the others appearing in the error analysis of the method. Although in general the dominant contribution to the extra error comes from $\mu\|\nabla \cdot (\boldsymbol{u}_h^n - \boldsymbol{u}^n)\|_0^2$, thanks to the use of grad–div stabilization the error $\mu\|\nabla \cdot (\boldsymbol{u}_h^n - \boldsymbol{u}^n)\|_0^2$ has the same rate of decay with h as the L^2 velocity error: $\|\boldsymbol{u} - \boldsymbol{u}_h\|_0^2$.

Theorem 4.2. *Let $\boldsymbol{u}$ be the velocity in the Navier–Stokes equations (1), let $\boldsymbol{u}_r$ be the grad–div POD stabilized approximation defined in (21), assume that the solution $(\boldsymbol{u}, p)$ of (1) is regular enough and condition (44) holds. Then, the error can be bounded as follows*

$$\begin{aligned}
\sum_{j=1}^{n} \Delta t \|\boldsymbol{u}_r^j - \boldsymbol{u}^j\|_0^2 \le 3Te^{2TC_u} &\left(\|\boldsymbol{e}_r^0\|_0^2 + CT(\nu+\mu)\|S^v\|_0 \sum_{k=r+1}^{d_v} \lambda_k \right. \\
&+ C(1+\mu^{-1}T)C(\boldsymbol{u}, p, l+1)^2 \left(h^{2l} + (\Delta t)^2\right) \\
&\left. + C\mu^{-1}h^{2l}T\||\boldsymbol{u}|^2\|_{L^\infty(H^l)} \right) + 3T \sum_{k=r+1}^{d_v} \lambda_k \\
&+ 3TC(\boldsymbol{u}, p, l+1)^2 \left(h^{2l} + (\Delta t)^2\right).
\end{aligned} \tag{46}$$

Proof. Since $\sum_{j=1}^{n} \Delta t \|\boldsymbol{e}_r^j\|_0^2 \le T \max_{1\le j\le n} \|\boldsymbol{e}_r^j\|_0^2$ and

$$\begin{aligned}
\sum_{j=1}^{n} \Delta t \|\boldsymbol{u}_r^j - \boldsymbol{u}^j\|_0^2 \le 3 &\left(\sum_{j=1}^{n} \Delta t \|\boldsymbol{e}_r^j\|_0^2 + \sum_{j=1}^{n} \Delta t \|P_r^v \boldsymbol{u}_h^j - \boldsymbol{u}_h^j\|_0^2 \right. \\
&\left. + \sum_{j=1}^{n} \Delta t \|\boldsymbol{u}_h^j - \boldsymbol{u}^j\|_0^2 \right),
\end{aligned}$$

from (45), (14) and (11) we easily obtain (46). □

Remark 4.3. We have chosen, as in [1], to analyze the concrete case in which the divergence form is used for the FOM method and the EMAC form is applied for the POD method but the error analysis of any other combination of discretizations of the nonlinear terms with analogous properties could be carried out in a similar way.

Remark 4.4. With the POD method defined in (21) we can obtain an approximation to the velocity but not to the pressure. In case an approximation to the pressure is also required one can use a supremizer pressure recovery

method. This procedure is analyzed in [2], see also [16]. One can argue exactly as in [2, Theorem 5.4] to get an error bound for the pressure, in which, as in Theorem 4.2, one will have to add to the error terms in [2, Theorem 5.4] those coming from the different discretizations used in the nonlinear terms (i.e. fourth and fifth terms on the right-hand side of (40)).

4.2. Error analysis of the method without grad–div stabilization

In this section we consider the case analyzed in [1] in which the plain Galerkin method is used instead of the grad–div stabilized method, i.e, we take $\mu = 0$ both in Eqs. (10) and (21).

In the following error analysis, as in [1], one does not get error bounds independent on inverse powers of the viscosity. The analysis can be obtained with slight modifications of the analysis of the previous section.

First, we notice that the last terms on each side of identity (27) are not present. Then, applying (3) in (38) to bound $\|\nabla\cdot\boldsymbol{e}_r^n\|_0$ by $\|\nabla\boldsymbol{e}_r^n\|_0$, instead of (39) we get

$$\begin{aligned}\frac{1}{2}|(|\boldsymbol{u}_h^n|^2,\nabla\cdot\boldsymbol{e}_r^n)| &\le \frac{1}{2}(\|\boldsymbol{u}^n\|_\infty + C_{\boldsymbol{u},\mathrm{inf}})\|\boldsymbol{u}^n-\boldsymbol{u}_h^n\|_0\|\nabla\cdot\boldsymbol{e}_r^n\|_0\\ &+\frac{1}{2}\|(I-P_{Q_h})|\boldsymbol{u}^n|^2\|_0\|\nabla\cdot\boldsymbol{e}_r^n\|_0 \le C\nu^{-1}(\|\boldsymbol{u}^n-\boldsymbol{u}_h^n\|_0^2+\|(I-P_{Q_h})|\boldsymbol{u}^n|^2\|_0^2)\\ &+\frac{\nu}{4}\|\nabla\cdot\boldsymbol{e}_r^n\|_0^2.\end{aligned} \tag{47}$$

Consequently, instead of (40) we obtain

$$\begin{aligned}|I| \le &\left(1+CC_{1,\mathrm{inf}}+\frac{1}{4}\right)\|\boldsymbol{e}_r^n\|_0^2+\frac{\nu}{4}\|\nabla\boldsymbol{e}_r^n\|_0^2\\ &+C\|\nabla\boldsymbol{\eta}_h^n\|_0^2+C\|\nabla\cdot(\boldsymbol{u}_h^n-\boldsymbol{u}^n)\|_0^2\\ &+C\nu^{-1}(\|\boldsymbol{u}-\boldsymbol{u}_h\|_0^2+\|(I-P_{Q_h})|\boldsymbol{u}^n|^2\|_0^2).\end{aligned}$$

Instead of (41) we can write

$$|II| \le \nu\|\nabla\boldsymbol{\eta}_h^n\|_0^2+\frac{\nu}{4}\|\nabla\boldsymbol{e}_r^n\|_0^2,$$

to conclude the following inequality instead of (43),

$$\begin{aligned}&\|\boldsymbol{e}_r^n\|_0^2+\nu\sum_{j=1}^n\Delta t\|\nabla\boldsymbol{e}_r^j\|_0^2\\ &\le \|\boldsymbol{e}_r^0\|_0^2+\sum_{j=1}^n\Delta t\left(5/4+CC_{1,\mathrm{inf}}\right)\|\boldsymbol{e}_r^j\|_0^2+C\nu\sum_{j=1}^n\Delta t\|\nabla\boldsymbol{\eta}_h^j\|_0^2\\ &+C\sum_{j=1}^n\Delta t\|\nabla\cdot(\boldsymbol{u}_h^j-\boldsymbol{u}^j)\|_0^2+C\nu^{-1}\sum_{j=1}^n\Delta t\|\boldsymbol{u}_h^j-\boldsymbol{u}^j\|_0^2\\ &+C\nu^{-1}\sum_{j=1}^n\Delta t\|(I-P_{Q_h})|\boldsymbol{u}^j|^2\|_0^2.\end{aligned} \tag{48}$$

From the above inequality one can argue exactly as before to conclude that, if

$$\Delta t C_u := \Delta t\left(5/4+CC_{1,\mathrm{inf}}\right) \le \frac{1}{2} \tag{49}$$

then, the following bound holds

$$\begin{aligned}\|\boldsymbol{e}_r^n\|_0^2+\nu\sum_{j=1}^n\Delta t\|\nabla\boldsymbol{e}_r^j\|_0^2 \le e^{2TC_u}&\left(\|\boldsymbol{e}_r^0\|_0^2+CT\nu\|S^v\|_0\sum_{k=r+1}^{d_v}\lambda_k\right.\\ &+CT(h^{-2}+\nu^{-1})C(\boldsymbol{u},p,\nu^{-1},l+1)^2\left(h^{2l+2}+(\Delta t)^2\right)\\ &\left.+C\nu^{-1}h^{2l}T\||\boldsymbol{u}|^2\|_{L^\infty(H^l)}\right),\end{aligned} \tag{50}$$

where we have applied (3) to bound the fourth term on the right-hand side of (48) and the error bound of the plain Galerkin method (12). From (50) and arguing as before we conclude

Theorem 4.5. *Let $\boldsymbol{u}$ be the velocity in the Navier–Stokes equations (1), let $\boldsymbol{u}_r$ be the grad–div POD approximation without stabilization (case $\mu = 0$) and assume that the solution $(\boldsymbol{u}, p)$ of (1) is regular enough. Then, assuming condition (49) holds, the error can be bounded as follows*

$$\begin{aligned}\sum_{j=1}^{n} \Delta t \|\boldsymbol{u}_r^j - \boldsymbol{u}^j\|_0^2 \le 3Te^{2TC_u} \Bigg(& \|\boldsymbol{e}_r^0\|_0^2 + CT\nu\|S^v\|_0 \sum_{k=r+1}^{d_v} \lambda_k \\ & + CT(h^{-2} + \nu^{-1})C(\boldsymbol{u}, p, \nu^{-1}, l+1)^2 \left(h^{2l+2} + (\Delta t)^2\right) \\ & + C\nu^{-1}h^{2l}T\||\boldsymbol{u}|^2\|_{L^\infty(H^l)}\Big) + 3T \sum_{k=r+1}^{d_v} \lambda_k \\ & + 3TC(\boldsymbol{u}, p, \nu^{-1}, l+1)^2 \left(h^{2l+2} + (\Delta t)^2\right). \end{aligned} \tag{51}$$

The final error bound depend explicitly on ν^{-1} and on both the L^2 error of the FOM velocity approximation and the error in the divergence of the FOM approximation (that we have bounded by the H^1 error).

Remark 4.6. Integrating by parts in (37) and applying (16), (17) and (2) we can bound

$$\begin{aligned}\frac{1}{2}((\nabla\cdot(\boldsymbol{u}^n - \boldsymbol{u}_h^n))\boldsymbol{u}_h^n, \boldsymbol{e}_r^n) \le & CC_{\boldsymbol{u},\mathrm{ld}}^2 \frac{\nu^{-1}}{4}\|\boldsymbol{u}^n - \boldsymbol{u}_h^n\|_0^2 + \frac{\nu}{4}\|\nabla\boldsymbol{e}_r^n\|_0^2 \\ & + C_{\boldsymbol{u},\inf}^2 \frac{\nu^{-1}}{4}\|\boldsymbol{u}^n - \boldsymbol{u}_h^n\|_0^2 + \frac{\nu}{4}\|\nabla\boldsymbol{e}_r^n\|_0^2.\end{aligned}$$

Arguing in this way, we remove the divergence term from (48) and, consequently, the factor h^{-2} in (50).

Remark 4.7. Alternatively, we can also bound the method without grad–div stabilization in a way that inverse constants of the viscosity do not appear explicitly in the constants. However, the error depends on the error of the plain Galerkin method (12) which in terms depend on ν^{-1}.

To this end, instead of (38), we can write, integrating by parts

$$\begin{aligned}&\frac{1}{2}(|\boldsymbol{u}_h^n|^2, \nabla\cdot\boldsymbol{e}_r^n)| \le \frac{1}{2}(|\boldsymbol{u}_h^n|^2 - |\boldsymbol{u}^n|^2, \nabla\cdot\boldsymbol{e}_r^n)| + \frac{1}{2}|(|\boldsymbol{u}^n|^2, \nabla\cdot\boldsymbol{e}_r^n)| \\ &= \frac{1}{2}|(\nabla\left(|\boldsymbol{u}_h^n|^2 - |\boldsymbol{u}^n|^2\right), \boldsymbol{e}_r^n)| + \frac{1}{2}|(\nabla\left((I - P_{Q_h})|\boldsymbol{u}^n|^2\right), \boldsymbol{e}_r^n)| \\ &\le C\|\boldsymbol{u}^n + \boldsymbol{u}_h^n\|_{1,\infty}\|\boldsymbol{u}^n - \boldsymbol{u}_h^n\|_1\|\boldsymbol{e}_r^n\|_0 + \frac{1}{2}\|(I - P_{Q_h})|\boldsymbol{u}^n|^2\|_1\|\boldsymbol{e}_r^n\|_0 \\ &\le C\left(\|\boldsymbol{u}^n - \boldsymbol{u}_h^n\|_1^2 + \|(I - P_{Q_h})|\boldsymbol{u}^n|^2\|_1^2\right) + \frac{1}{2}\|\boldsymbol{e}_r^n\|_0^2.\end{aligned}$$

Then, applying (3), instead of (40) we get

$$\begin{aligned}|I| \le & \left(1 + CC_{1,\inf}\right)\|\boldsymbol{e}_r^n\|_0^2 + C\|\nabla\boldsymbol{\eta}_h^n\|_0^2 + C\|\boldsymbol{u}_h^n - \boldsymbol{u}^n\|_1^2 \\ & + C(\|(I - P_{Q_h})|\boldsymbol{u}^n|^2\|_1^2),\end{aligned}$$

and then, for $C_u = 1 + CC_{1,\inf}$ and $\Delta t C_u \le 1/2$, we conclude

$$\begin{aligned}\|\boldsymbol{e}_r^n\|_0^2 + \nu\sum_{j=1}^{n}\Delta t\|\nabla\boldsymbol{e}_r^j\|_0^2 \le e^{2TC_u}\Bigg(& \|\boldsymbol{e}_r^0\|_0^2 + CT\nu\|S^v\|_0\sum_{k=r+1}^{d_v}\lambda_k \\ & + CTC(\boldsymbol{u}, p, \nu^{-1}, l+1)^2h^{-2}\left(h^{2l+2} + (\Delta t)^2\right) \\ & + Ch^{2(l-1)}T\||\boldsymbol{u}|^2\|_{L^\infty(H^l)}\Big).\end{aligned}$$

As pointed out in [14], from the above error bound we observe that the grad–div stabilization could be suppressed when we use the EMAC form of the nonlinear term in the ROM method and we can still obtain error bounds with

constants independent on inverse powers of ν, apart from the dependence thought the error of the plain Galerkin method. However, the price to be paid is a lower rate of convergence. Compare the last term on the right-hand side above with (46). The rate of convergence obtained with this argument is also lower than the bound (51).

Remark 4.8. Let us observe that using divergence free elements in the FOM method (Scott–Vogelius [17], Neilan–Falk [18]) the ROM method heritages the divergence free property and all the different formulations for the nonlinear term are equivalent. This means that there is no discrepancy in the nonlinear terms in that case. As stated in [19], this case could be seen as the limit of Taylor–Hood elements with grad–div stabilization for $\mu \to \infty$ assuming a mesh for which Scott–Vogelius pair is inf–sup stable, since in that case the sequence of velocity solutions for the Taylor–Hood pair with grad–div stabilization converges to the velocity solution of the Galerkin method for the Scott–Vogelius pair. On the other hand, the case $\mu = 0$ corresponds to the case analyzed in this section for the method without grad–div stabilization. The intermediate case, $0 < \mu < \infty$ has been analyzed in Section 4.1 and there is an extra error term coming from using different discretizations of the nonlinear term in the FOM and ROM methods, respectively, which decreases, accordingly to the above comments, as μ increases.

5. Numerical experiments

In this section, we present numerical results for the grad–div reduced order model (ROM) (21), introduced and analyzed in the previous section. Actually, a comparison is performed by using both the skew-symmetric (9) and the EMAC (22) form for the discretization of the nonlinear term at ROM level. In this context, also different offline/online values of the grad–div stabilization parameter μ are tested.

For comparison purposes, we repeat the numerical experiments without grad–div stabilization, as in [1], for which the error analysis performed in Section 4.2 holds.

The numerical experiments are performed on the benchmark problem of the 2D unsteady flow around a cylinder with circular cross-section [20] at Reynolds number $Re = 100$ ($\nu = 10^{-3}\,\mathrm{m}^2/\mathrm{s}$). The open-source FE software FreeFEM [21] has been used to run the numerical experiments, following the setup from [2].

FOM and POD modes. The numerical method used to compute the snapshots for the grad–div-ROM (21) is the grad–div finite element method (FEM) (8) described in Section 2, with the skew-symmetric form (9) of the nonlinear term. A spatial discretization using the Hood–Taylor MFE pair $\mathbf{P}^2 - \mathbb{P}^1$ for velocity–pressure is considered on a relatively coarse computational grid (see [2]), for which $h = 2.76 \cdot 10^{-2}\,\mathrm{m}$, resulting in 32 488 d.o.f. for velocities and 4 151 d.o.f. for pressure.

As in [2], for the time discretization, a semi-implicit Backward Differentiation Formula of order two (BDF2) has been applied (see [22] for further details), with time step $\Delta t = 2 \cdot 10^{-3}\,\mathrm{s}$. Time integration is performed until a final time $T = 15\,\mathrm{s}$. In the time period $[0, 5]\,\mathrm{s}$, after an initial spin-up, the flow is expected to develop to full extent, including a subsequent relaxation time. Afterwards, it reaches a periodic-in-time (statistically- or quasi-steady) state.

The POD modes are generated in L^2 by the method of snapshots with velocity centered-trajectories [23] by storing every FOM solution from $t = 5\,\mathrm{s}$, when the solution had reached a periodic-in-time state, and just using one period of snapshot data. The full period length of the statistically steady state is 0.332 s, thus we collect 167 velocity snapshots to generate the POD basis $\boldsymbol{U}^r$.

With the same strategy, we repeat the numerical experiments without grad–div stabilization, as in [1], so that in this case we use the FOM (8) with $\mu = 0$ to compute the snapshots for the construction of the POD modes.

In Section 5.1, we discuss numerical results for grad–div-ROM with different discretization of the nonlinear term, but using in the online phase the same grad–div stabilization parameter μ used in the offline phase. In Section 5.2, we repeat this test by using in the online phase a different grad–div stabilization parameter μ_{on} w.r.t. the one used in the offline phase. Finally, in Section 5.3, we turn off the grad–div stabilization both in the offline and in the online phase, as in [1].

5.1. Numerical results for grad–div-ROM with different discretization of the nonlinear term

With POD velocity modes generated, the fully discrete grad–div-ROM (21) is constructed as discussed in the previous section, using the semi-implicit BDF2 time scheme as for the FOM, and run with both skew-symmetric (as for the FOM) and EMAC (different from the FOM) formulation of the nonlinear term in the stable response time interval $[5, 15]\,\mathrm{s}$ with $\Delta t = 2 \cdot 10^{-3}\,\mathrm{s}$. In this case, the value used as grad–div stabilization parameter for the ROM

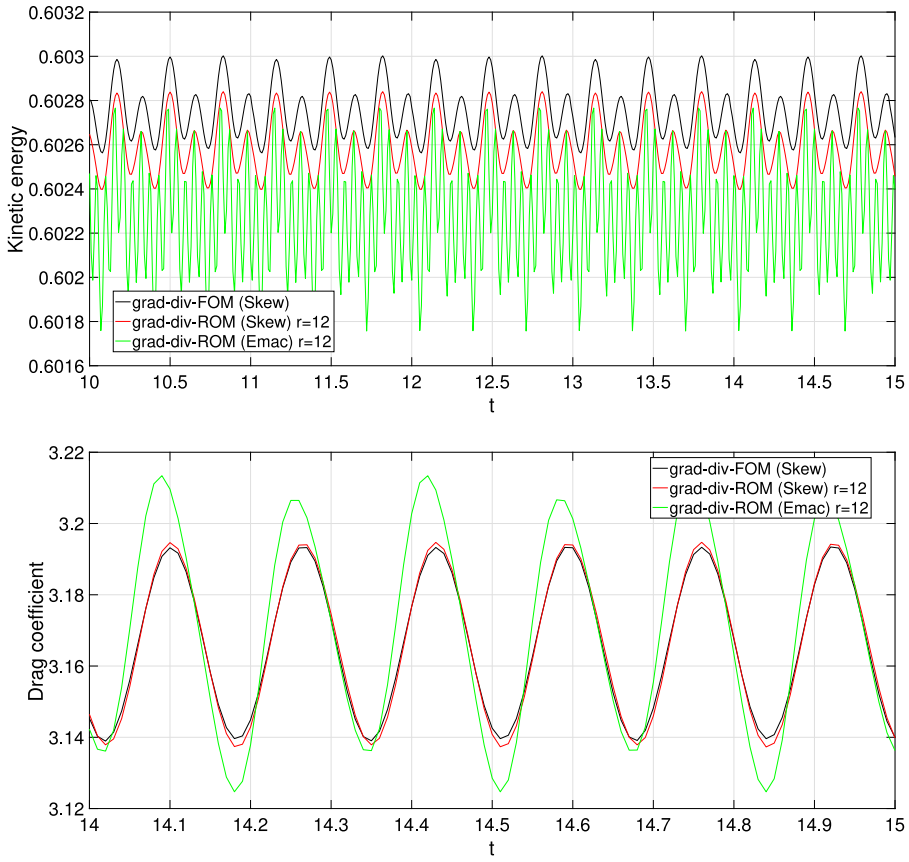

Fig. 1. Temporal evolution of kinetic energy (top) and drag coefficient (bottom) computed with grad–div-ROM (21) using $r = 12$ velocity modes. Comparison with grad–div-FOM (8).

is the same used for the FOM, that is $\mu = 10^{-2}$. The initial reduced-order velocity is given by the L^2-orthogonal projection P_r^v of the velocity snapshot at $t = 5$ s on the POD velocity space $\boldsymbol{U}^r$.

For this first numerical experiment, the temporal evolution of the local drag coefficient and kinetic energy are monitored and compared to the FOM solutions in the predictive time interval [10, 15] s, for which the quantities of interest stabilizes for all methods (for ease of comparison, drag is shown only on the last part of the time interval [14, 15] s). To compute drag coefficient, we used the volume integral formulation from [24], where the pressure term is not necessary if the test function is taken properly in the discrete divergence-free space $\boldsymbol{V}_{h,l}$ (4) (by Stokes projection, for instance), as done in [25,26].

Numerical results for kinetic energy and drag predictions using $r = 12$ velocity modes are shown in Fig. 1, where we display a comparison of grad–div-FOM (8) with the skew-symmetric form of the nonlinear term, and grad–div-ROM (21) with both skew-symmetric and EMAC form of the nonlinear term.

From this figure, we see that the grad–div-ROM with the skew-symmetric form of the nonlinear term (as for the FOM) gives better results for both kinetic energy and drag predictions. The good match that we observe using the same discretization for the nonlinear term as for the FOM (Skew) is slightly degraded using a different formulation of the nonlinear term (EMAC) in the online phase, as predicted by the theoretical study.

To further assess the numerical accuracy of the grad–div-ROM (21) with both skew-symmetric and EMAC form of the nonlinear term, numerical results for kinetic energy and drag predictions varying r, i.e. the number of velocity modes, are shown in Figs. 2 and 3, respectively, where we display a comparison to grad–div-FOM (8) with the skew-symmetric form of the nonlinear term. From these results, we can check again that better results are obtained

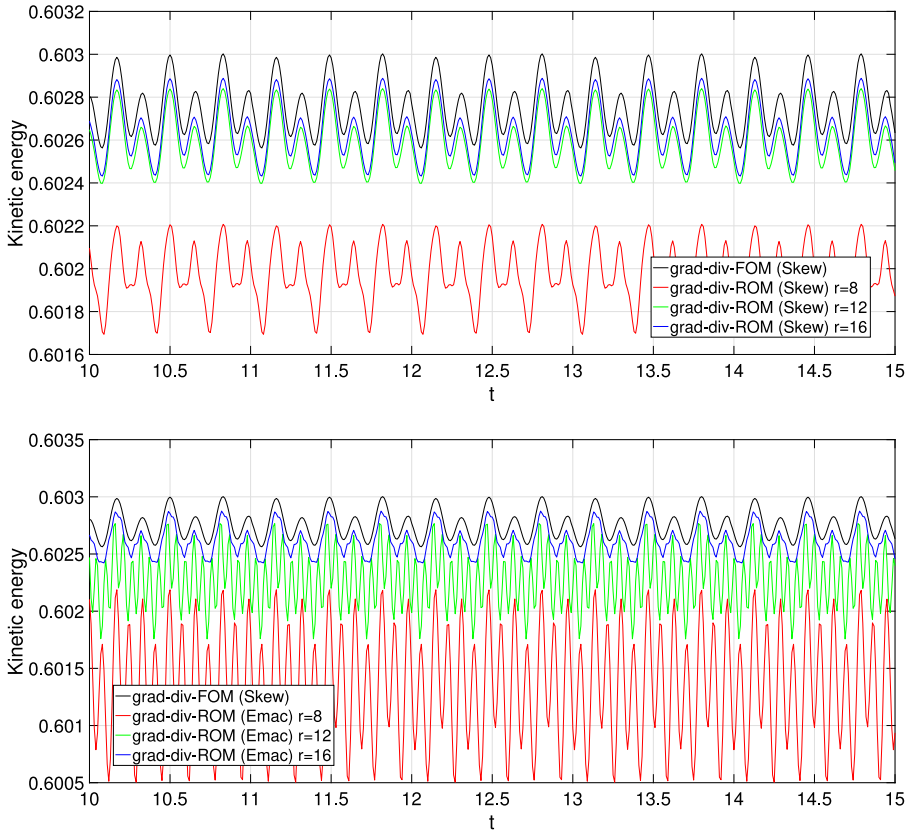

Fig. 2. Temporal evolution of kinetic energy computed with grad–div-ROM (21) (Skew, top; Emac, bottom) using $r = 8, 12, 16$ velocity modes. Comparison with grad–div-FOM (8).

when using the grad–div-ROM with the skew-symmetric form of the nonlinear term (as for the FOM). In agreement with our theoretical analysis, we can observe a reduction of the ROM error when increasing r for both forms of the nonlinear term. In case of using a different formulation of the nonlinear term (EMAC) in the online phase the difference to the FOM solution is bigger, due to the extra error term, as the analysis predicts.

5.2. Numerical results for grad–div-ROM with different discretization of the nonlinear term and stabilization coefficient

In this section, we are interested in numerically investigate how the value of the grad–div stabilization parameter influences the results. For this purpose, we perform numerical experiments considering a larger value of the online grad–div stabilization parameter ($\mu_{\text{on}} = 1$) with respect to the one used for offline computations ($\mu_{\text{off}} = 10^{-2}$), and repeat the previous computations. We observed that this parameter influences especially the sensitive local quantity of drag coefficient, so that we show results for its temporal evolution.

In Fig. 4, numerical results for drag predictions using $r = 12$ velocity modes are displayed. From this figure, we see that, independently of the online form of the nonlinear term, larger differences are present with respect to the previous results.

Also, if we vary the number of velocity modes, as done in Fig. 5, we observe that in this context we do not get convergence in any case by increasing r. The explanation for this behavior is as follows. When using different values for the grad–div parameter in the offline, μ_{off}, and online computations, μ_{on}, there is an extra term in the error of size $|\mu_{\text{on}} - \mu_{\text{off}}|^{1/2}\|\nabla \cdot \boldsymbol{u}_h\|_0$. In Fig. 6 we have plotted the strong ($\|\nabla \cdot \boldsymbol{u}_h\|_0$) and weak ($\max_{q_h \in Q_h} |(\nabla \cdot \boldsymbol{u}_h, q_h)|/\|q_h\|_0$)

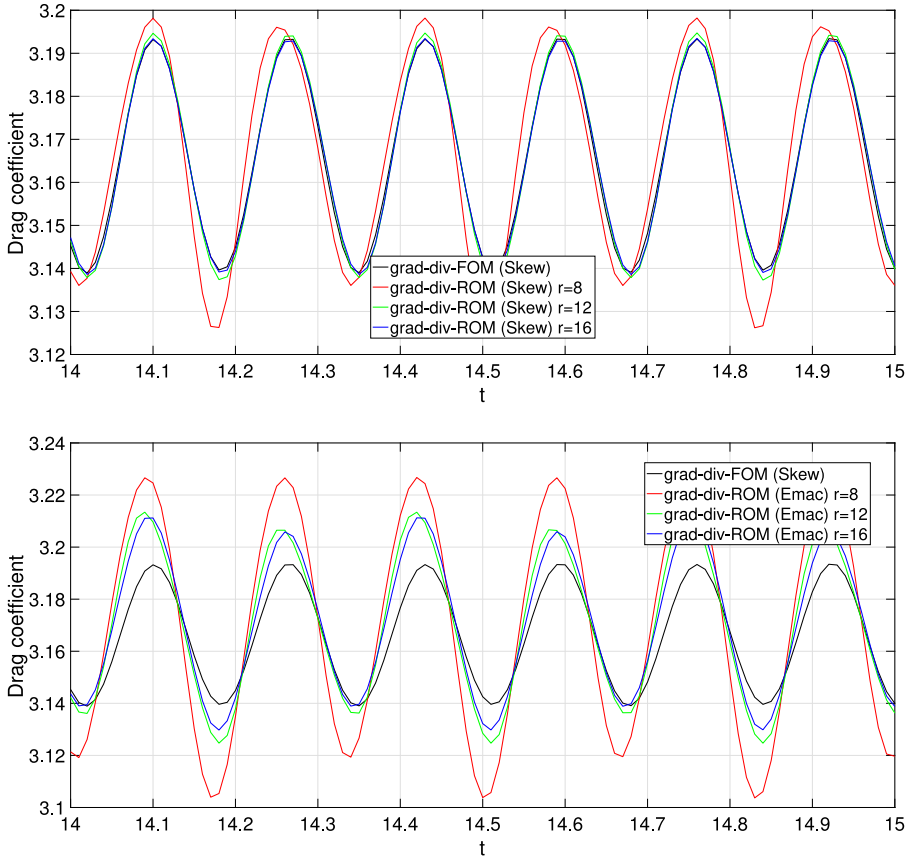

Fig. 3. Temporal evolution of drag coefficient computed with grad–div-ROM (21) (Skew, top; Emac, bottom) using $r = 8, 12, 16$ velocity modes. Comparison with grad–div-FOM (8).

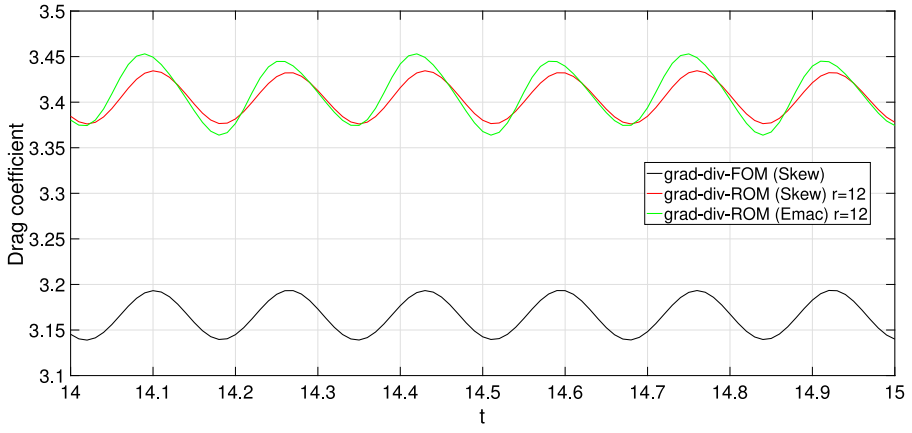

Fig. 4. Temporal evolution of drag coefficient computed with grad–div-ROM (21) with $\mu_{\rm on} = 1$ using $r = 12$ velocity modes. Comparison with grad–div-FOM (8).

divergence of $\boldsymbol{u}_h$. We can observe that while the weak divergence is essentially zero the strong divergence is quite large. Since in the experiment the value $|\mu_{\rm on} - \mu_{\rm off}| = 0.99$, this means that the extra error has size approximately

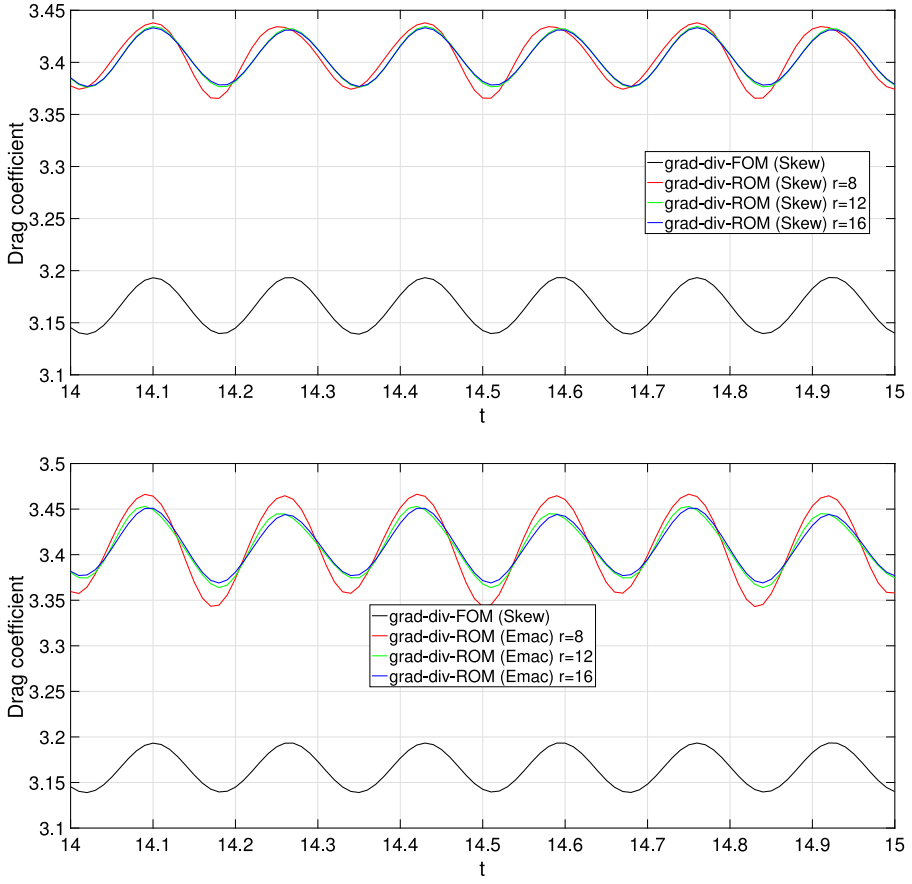

Fig. 5. Temporal evolution of drag coefficient computed with grad–div-ROM (21) (Skew, top; Emac, bottom) with $\mu_{\text{on}} = 1$ using $r = 8, 12, 16$ velocity modes. Comparison with grad–div-FOM (8).

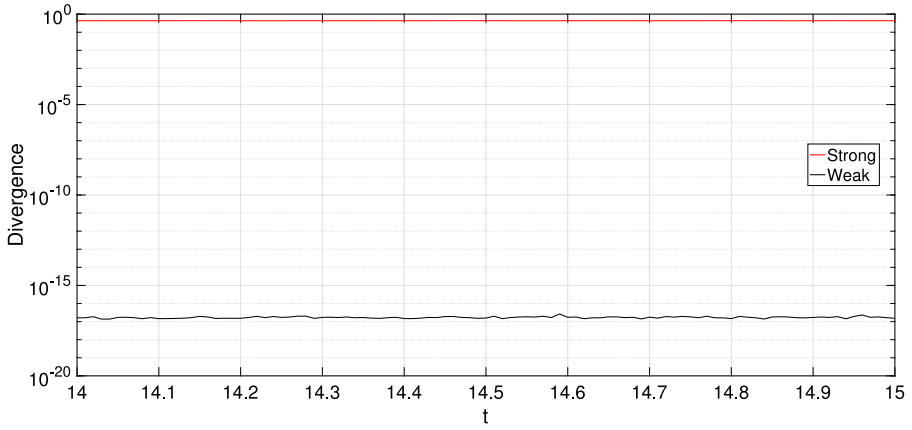

Fig. 6. Temporal evolution of the strong (red) and weak (black) divergence of $\boldsymbol{u}_h$. (For interpretation of the references to color in this figure legend, the reader is referred to the web version of this article.)

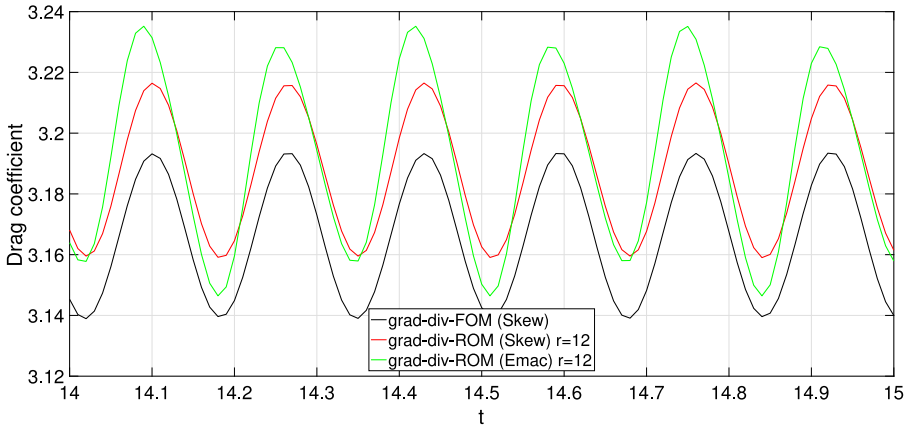

Fig. 7. Temporal evolution of drag coefficient computed with grad–div-ROM (21) with $\mu_{\text{on}} = 0.1$ using $r = 12$ velocity modes. Comparison with grad–div-FOM (8).

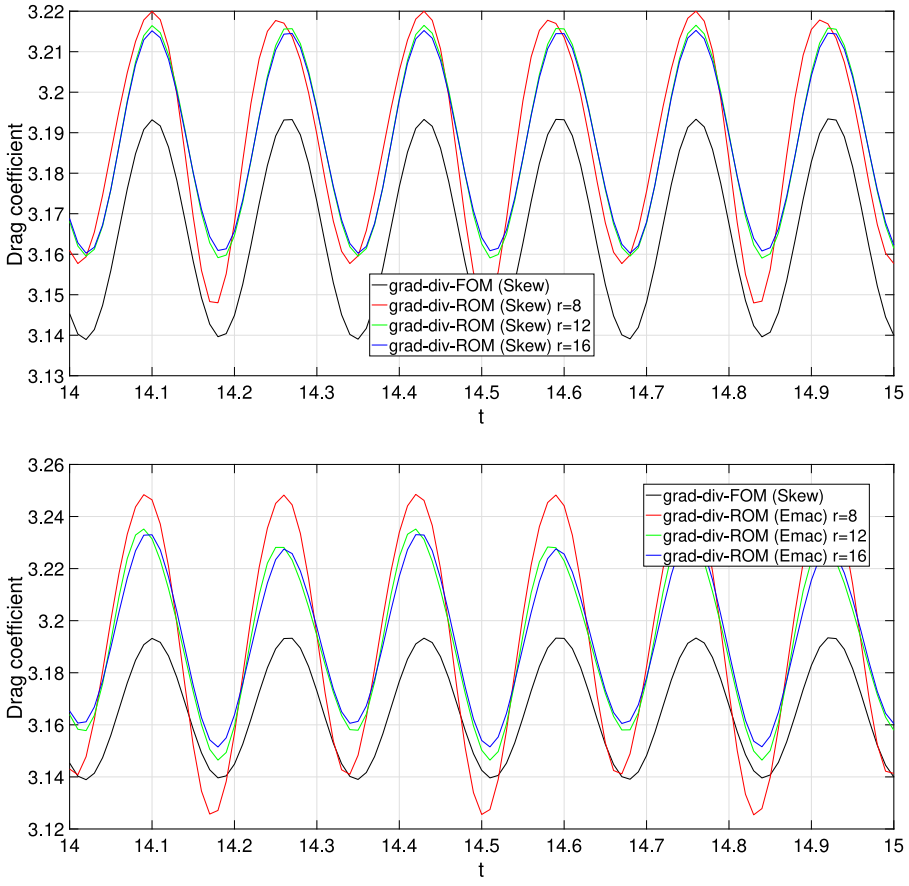

Fig. 8. Temporal evolution of drag coefficient computed with grad–div-ROM (21) (Skew, top; Emac, bottom) with $\mu_{\text{on}} = 0.1$ using $r = 8, 12, 16$ velocity modes. Comparison with grad–div-FOM (8).

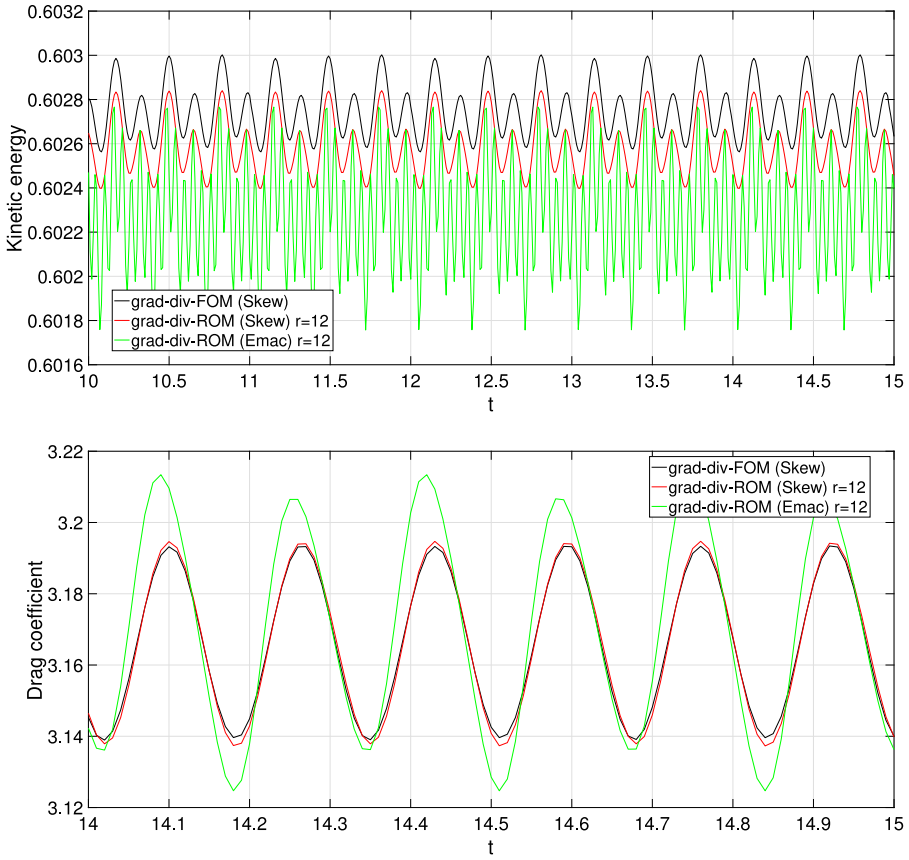

Fig. 9. Temporal evolution of kinetic energy (top) and drag coefficient (bottom) computed with ROM (21) ($\mu = 0$) using $r = 12$ velocity modes. Comparison with FOM (8) ($\mu = 0$).

equal to the value $\|\nabla \cdot \boldsymbol{u}_h\|_0$ which is considerably big, explaining the big difference between the FOM values of the drag coefficient compared to the ROM values.

To support the above explanation we now repeat Figs. 4 and 5 with $\mu_{\text{on}} = 0.1$. In this case the difference $|\mu_{\text{on}} - \mu_{\text{off}}|$ is divided by around 10 and $|\mu_{\text{on}} - \mu_{\text{off}}|^{1/2}$ is 0.3. In Figs. 7 and 8 we have plotted the results. While in Figs. 4 and 5 the error in the drag coefficients has the size of $\|\nabla \cdot \boldsymbol{u}_h\|_0$, in Figs. 7 and 8 this error has size 0.3 times $\|\nabla \cdot \boldsymbol{u}_h\|_0$ (the error is divided by 3.3 approximately respect to the previous experiment as can be observed). Since the error $|\mu_{\text{on}} - \mu_{\text{off}}|^{1/2}\|\nabla \cdot \boldsymbol{u}_h\|_0$ is smaller than before, in Fig. 8 we can now observe some improvement while increasing the number of modes. The improvement is bigger from $r = 8$ to $r = 12$ than from $r = 12$ to $r = 16$ since once the error reaches the quantity $|\mu_{\text{on}} - \mu_{\text{off}}|^{1/2}\|\nabla \cdot \boldsymbol{u}_h\|_0$, no further reduction of the errors is expected.

5.3. Numerical results for ROM without grad–div and different discretization of the nonlinear term

Finally, as in [1], we repeat the numerical experiments of Section 5.1 without grad–div stabilization, for which the error analysis performed in Section 4.2 holds. In particular, we use the FOM (8) with $\mu = 0$ to compute the snapshots for the construction of the POD modes. With POD velocity modes generated, the fully discrete ROM (21) with $\mu = 0$ is run with both skew-symmetric (as for the FOM) and EMAC (different from the FOM) formulation of the nonlinear term.

Numerical results for kinetic energy and drag predictions using $r = 12$ velocity modes are shown in Fig. 9, where we display a comparison of FOM (8) ($\mu = 0$) with the skew-symmetric form of the nonlinear term, and ROM (21) ($\mu = 0$) with both skew-symmetric and EMAC form of the nonlinear term.

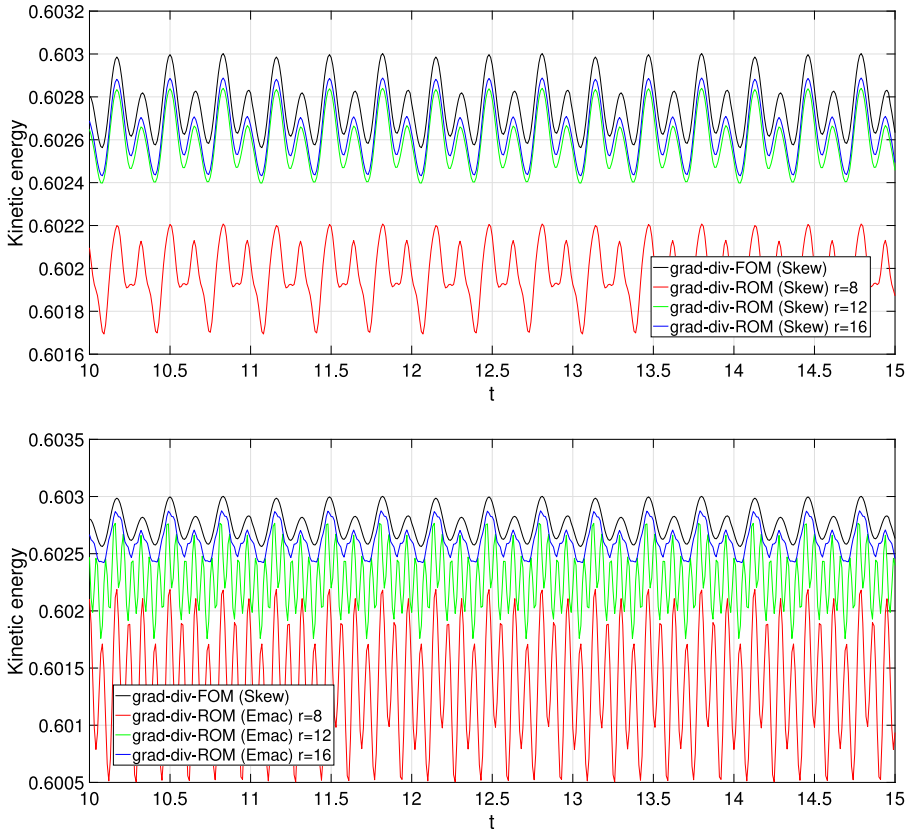

Fig. 10. Temporal evolution of kinetic energy computed with ROM (21) (Skew, top; Emac, bottom; $\mu = 0$) using $r = 8, 12, 16$ velocity modes. Comparison with FOM (8) ($\mu = 0$).

From this figure, similarly to Section 5.1 and in agreement with [1], we see again that the ROM with the skew-symmetric form of the nonlinear term (as for the FOM) gives better results for both kinetic energy and drag predictions, in the sense that the good match that we observe using the same discretization for the nonlinear term as for the FOM (Skew) is slightly degraded using a different formulation of the nonlinear term (EMAC) in the online phase, as predicted by the theoretical study.

Also in this context, we show numerical results for kinetic energy and drag predictions varying r, i.e. the number of velocity modes, in Figs. 10 and 11, respectively, where we display a comparison to FOM (8) ($\mu = 0$) with the skew-symmetric form of the nonlinear term. From these results, similarly to Section 5.1, we can again observe that better results are obtained when using the ROM with the skew-symmetric form of the nonlinear term (as for the FOM). In view of Remark 4.6, we can avoid the appearance of the term $\|\nabla \cdot (\boldsymbol{u}_h - \boldsymbol{u})\|_0$ in the error analysis having instead the term $\nu^{-1/2}\|\boldsymbol{u}_h - \boldsymbol{u}\|_0$. Since $\nu^{-1/2} \approx 31.6$ in this experiment this extra term is still small and, consequently, we can observe a reduction of the ROM error when increasing r with both nonlinear terms, although the reduction is larger when the same term is used in the FOM and ROM methods. We want to remark that, in case of using a coarser mesh to compute the FOM approximation and/or a bigger Reynolds number, the error term: $\min(\nu^{-1/2}\|\boldsymbol{u}_h - \boldsymbol{u}\|_0, \|\nabla \cdot (\boldsymbol{u}_h - \boldsymbol{u})\|_0)$ could dominate the behavior of the ROM approximation giving no improvement while increasing the number of modes, see the numerical experiments in [1].

6. Conclusions

As a conclusion, we can say that there are extra error terms in the case in which different discretizations are used for the nonlinear terms in the FOM and POD methods. Although these extra error terms lead in general to a less accurate method, in many examples, specially in the case in which grad–div stabilization is used, the extra error is small and the non consistent FOM–ROM method can still be used in practice.

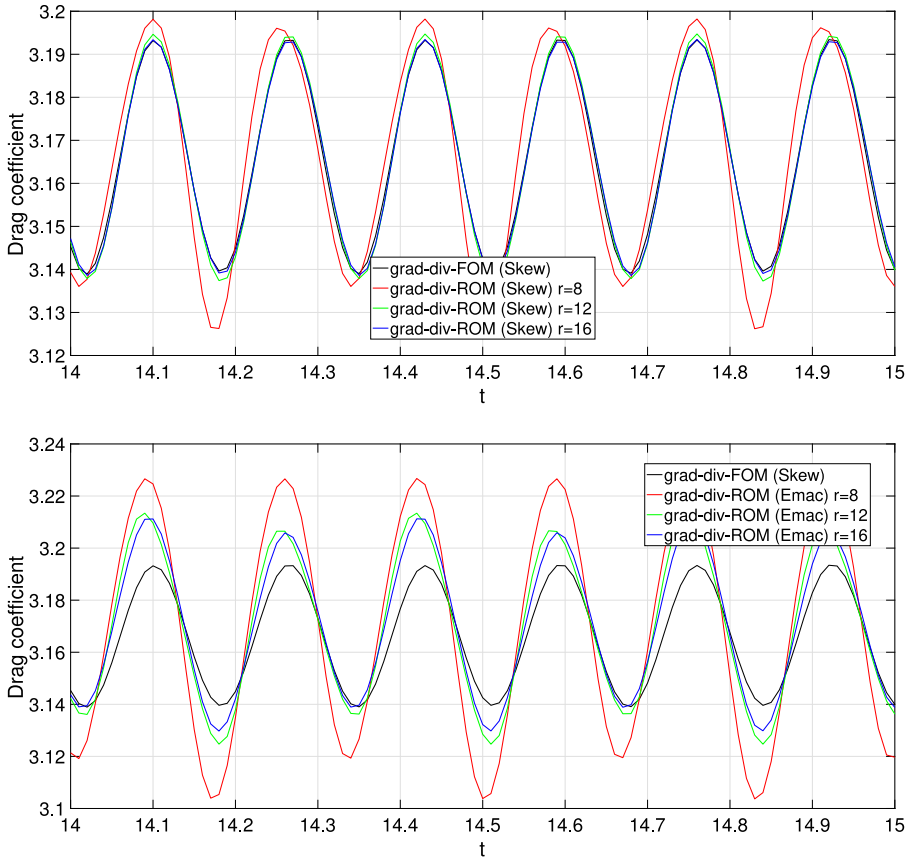

Fig. 11. Temporal evolution of drag coefficient computed with ROM (21) (Skew, top; Emac, bottom; $\mu = 0$) using $r = 8, 12, 16$ velocity modes. Comparison with FOM (8) ($\mu = 0$).

In the case in which grad-did stabilization is added to both the FOM and POD methods error bounds with constants independent on inverse powers of the viscosity can be obtained. Comparing the case in which the same discretization of the nonlinear term is used for both FOM and POD methods we have bounded the added term in the error that has the size of the error of the FOM method (in the L^2 norm of the velocity and the L^2 norm of the divergence of the velocity).

On the other hand, in the case in which no stabilization is added neither to the FOM nor to the POD method, we have carried out two different error analysis. In the first one, the error bounds depend on inverse powers of the viscosity and on the L^2 error of the velocity and the L^2 error of the divergence of the velocity of the FOM method plus the L^2 error of the projection of the square modulus of the velocity onto the FEM pressure space. In the second one, we are able to prove error bounds with constants independent on inverse powers of the viscosity but with the price of having bounds that depend on the H^1 norm of the FEM velocity error and the H^1 error of the projection of the square modulus of the velocity onto the FEM pressure space. Moreover, since the bounds for the plain Galerkin method depend on inverse powers of the viscosity the dependence on ν^{-1} cannot completely be avoided also in this case.

Overall, we have identified all the terms in the error bounds for different combinations of discretizations of the nonlinear term adding or not grad–div stabilization.

Declaration of competing interest

The authors declare that they have no known competing financial interests or personal relationships that could have appeared to influence the work reported in this paper.

Data availability

No data was used for the research described in the article.

References

[1] S. Ingimarson, L.G. Rebholz, T. Iliescu, Full and reduced order model consistency of the nonlinearity discretization in incompressible flows, Comput. Methods Appl. Mech. Engrg. 401 (part B) (2022) 16, Paper No. 115620.
[2] J. Novo, S. Rubino, Error analysis of proper orthogonal decomposition stabilized methods for incompressible flows, SIAM J. Numer. Anal. 59 (1) (2021) 334–369.
[3] S. Charnyi, T. Heister, M.A. Olshanskii, L.G. Rebholz, On conservation laws of Navier-Stokes Galerkin discretizations, J. Comput. Phys. 337 (2017) 289–308.
[4] S. Charnyi, T. Heister, M.A. Olshanskii, L.G. Rebholz, Efficient discretizations for the EMAC formulation of the incompressible Navier-Stokes equations, Appl. Numer. Math. 141 (2019) 220–233.
[5] R.A. Adams, Sobolev Spaces, in: Pure and Applied Mathematics, vol. 65, Academic Press, New York-London, 1975, [A subsidiary of Harcourt Brace Jovanovich, Publishers].
[6] V. John, Finite Element Methods for Incompressible Flow Problems, in: Springer Series in Computational Mathematics, vol. 51, Springer, Cham, 2016.
[7] P.G. Ciarlet, The Finite Element Method for Elliptic Problems, in: Classics in Applied Mathematics, vol. 40, Society for Industrial and Applied Mathematics (SIAM), Philadelphia, PA, 2002, Reprint of the 1978 original [North-Holland, Amsterdam; MR0520174 (58 #25001)].
[8] F. Brezzi, R.S. Falk, Stability of higher-order Hood-Taylor methods, SIAM J. Numer. Anal. 28 (3) (1991) 581–590.
[9] C. Taylor, P. Hood, A numerical solution of the Navier-Stokes equations using the finite element technique, Internat. J. Comput. Fluids 1 (1) (1973) 73–100.
[10] J. de Frutos, B. García-Archilla, V. John, J. Novo, Analysis of the grad-div stabilization for the time-dependent Navier-Stokes equations with inf-sup stable finite elements, Adv. Comput. Math. 44 (1) (2018) 195–225.
[11] K. Kunisch, S. Volkwein, Galerkin proper orthogonal decomposition methods for parabolic problems, Numer. Math. 90 (1) (2001) 117–148.
[12] S. Ingimarson, An energy, momentum, and angular momentum conserving scheme for a regularization model of incompressible flow, J. Numer. Math. 30 (1) (2022) 1–22.
[13] M.A. Olshanskii, L.G. Rebholz, Longer time accuracy for incompressible Navier-Stokes simulations with the EMAC formulation, Comput. Methods Appl. Mech. Engrg. 372 (2020) 113369, 17.
[14] B. García-Archilla, V. John, J. Novo, On the convergence order of the finite element error in the kinetic energy for high Reynolds number incompressible flows, Comput. Methods Appl. Mech. Engrg. 385 (2021) 54, Paper No. 114032.
[15] J.G. Heywood, R. Rannacher, Finite-element approximation of the nonstationary Navier-Stokes problem. IV. Error analysis for second-order time discretization, SIAM J. Numer. Anal. 27 (2) (1990) 353–384.
[16] K. Kean, M. Schneier, Error analysis of supremizer pressure recovery for POD based reduced-order models of the time-dependent Navier-Stokes equations, SIAM J. Numer. Anal. 58 (4) (2020) 2235–2264.
[17] L.R. Scott, M. Vogelius, Conforming finite element methods for incompressible and nearly incompressible continua, in: Large-Scale Computations in Fluid Mechanics, Part 2 (La Jolla, Calif., 1983), in: Lectures in Appl. Math., vol. 22, Amer. Math. Soc., Providence, RI, 1985, pp. 221–244.
[18] R.S. Falk, M. Neilan, Stokes complexes and the construction of stable finite elements with pointwise mass conservation, SIAM J. Numer. Anal. 51 (2) (2013) 1308–1326.
[19] M.A. Case, V.J. Ervin, A. Linke, L.G. Rebholz, A connection between Scott-Vogelius and grad-div stabilized Taylor-Hood FE approximations of the Navier-Stokes equations, SIAM J. Numer. Anal. 49 (4) (2011) 1461–1481.
[20] M. Schäfer, S. Turek, Benchmark computations of laminar flow around a cylinder, in: E.H. Hirschel (Ed.), Flow Simulation with High-Performance Computers II, in: Notes on Numerical Fluid Mechanics, vol. 48, Vieweg, 1996, pp. 547–566.
[21] F. Hecht, New development in freefem++, J. Numer. Math. 20 (3–4) (2012) 251–265.
[22] N. Ahmed, S. Rubino, Numerical comparisons of finite element stabilized methods for a 2D vortex dynamics simulation at high Reynolds number, Comput. Methods Appl. Mech. Engrg. 349 (2019) 191–212.
[23] S. Giere, T. Iliescu, V. John, D. Wells, SUPG reduced order models for convection-dominated convection–diffusion-reaction equations, Comput. Methods Appl. Mech. Engrg. 289 (2015) 454–474.
[24] V. John, Reference values for drag and lift of a two-dimensional time-dependent flow around a cylinder, Internat. J. Numer. Methods Fluids 44 (2004) 777–788.
[25] B. García-Archilla, J. Novo, S. Rubino, Error analysis of proper orthogonal decomposition data assimilation schemes with grad-div stabilization for the Navier-Stokes equations, J. Comput. Appl. Math. 411 (2022) 30, Paper No. 114246.
[26] C. Zerfas, L.G. Rebholz, M. Schneier, T. Iliescu, Continuous data assimilation reduced order models of fluid flow, Comput. Methods Appl. Mech. Engrg. 357 (2019) 112596, 18.